Quaternary Science Reviews 311 (2023) 108136

Contents lists available at ScienceDirect

Quaternary Science Reviews

journal homepage: www.elsevier.com/locate/quascirev

Did the Eurasian ice sheets melt completely in early Marine Isotope Stage 3? New evidence from Norway and a synthesis for Eurasia

Jan Mangerud [a, *], Helena Alexanderson [b], Hilary H. Birks [c], Aage Paus [c], Zoran M. Perić [b], John Inge Svendsen [a]

[a] Department of Earth Science and Bjerknes Centre for Climate Research, University of Bergen, Norway
[b] Department of Geology, Lund University, Sweden
[c] Department of Biological Sciences and Bjerknes Centre for Climate Research, University of Bergen, Norway

ARTICLE INFO

Article history:
Received 1 March 2023
Received in revised form
7 May 2023
Accepted 15 May 2023
Available online 25 May 2023

Handling Editor: C. O'Cofaigh

Keywords:
Pleistocene
Weichselian
Last ice age
Glaciation
Sea level changes
Europe
Scandinavia
Luminescence dating
MIS 4
MIS 3

ABSTRACT

We describe glaci-lacustrine sediments buried under thick tills in Folldalen, south-east Norway, a site located close to the former centre of the Scandinavian Ice Sheet. Thus, the location implies that the ice sheet had melted when the sediments were deposited. The exposed ground was occupied by arctic vegetation. The best age estimate from 20 quartz luminescence dates is 55.6 ± 4.6 ka. Due to possible incomplete bleaching, an age in the younger part of the time range is most probable. We conclude that the Scandinavian Ice Sheet melted almost completely away early in Marine Isotope Stage (MIS) 3. Our review shows that the other Eurasian ice sheets also disappeared in that period. In north-western Germany, there were forests, containing warmth-demanding trees early in MIS 3, indicating a summer climate only slightly cooler than at present, thus supporting the evidence that the adjacent ice sheets had melted. The melting of the Eurasian ice sheets contributed to 50–100% of the sea-level rise from MIS 4 to MIS 3, implying that the much larger North American ice sheets did not melt much. In contrast, the Eurasian ice sheets contributed only about 30% to the sea-level drop from MIS 3 to MIS 2, meaning that the North American ice sheets during that period expanded strongly.

1. Introduction

Ice sheets function both as monitors of climate change and as strong players in the climate system. They cover large areas and form high mountains of ice influencing atmospheric circulation and increasing global albedo. Furthermore, they control the major global sea level changes, re-direct rivers, and occupy large shallow marine areas. Yet, field observations documenting pre-Last Glacial Maximum (LGM) ice-sheet fluctuations are sparse because glacial erosion during the LGM removed most of the older sediments, and remnant sediments became deeply buried. It is also difficult to obtain precise age estimates for such sediments.

The youngest pre-LGM period for considerable glacial retraction is Marine Isotope Stage (MIS) 3, between the two global glacial maxima at MIS 4 (75–60/57 ka) and the peak of MIS 2 (25–20 ka BP) Gowan et al. (2021); Kleman et al. (2021). We show in section 5.6 that it has previously been demonstrated that the Barents-Kara (Alexanderson et al., 2018; Ingólfsson and Landvik, 2013; Mangerud et al., 1998) and British (Finlayson et al., 2010) ice sheets probably melted completely during MIS 3. The Scandinavian Ice Sheet is by far the largest constituent of the Eurasian Ice Sheet Complex (Hughes et al., 2016), and the age and extent of the MIS 3 minimum size of this ice sheet is therefore crucial for reconstruction of the entire Eurasian Ice Sheet. A parallel discussion of MIS 3 ice-sheet extent is ongoing in North America (Dalton et al., 2022; Miller and Andrews, 2019).

A major review and evaluation of potential MIS-3-age sediment records in Scandinavia by Wohlfarth (2010) concluded that most of Sweden was ice free 60–35 ka BP, but acknowledged that the ages of most of the assessed deposits were problematic. Some additional

* Corresponding author. Department of Geoscience and Bjerknes Centre for Climate Research, University of Bergen, PO Box 7803, 5020, Bergen, Norway.
E-mail address: jan.mangerud@uib.no (J. Mangerud).

https://doi.org/10.1016/j.quascirev.2023.108136

sites are mentioned in an overview article about Norway by Olsen et al. (2013). More recently, Kleman et al. (2021) also maintained that there is solid evidence for ice free conditions in central Scandinavia during Early MIS 3 (about 55 ka), and they postulate a 20,000 years long ice-free period 55–35 ka before the ice sheet once again covered the entire country. Alexanderson et al. (2022) convincingly dated the glacially overrun Veiki moraine in northern Sweden to MIS 3, in contrast to earlier assumptions of a MIS 5c age (Fig. 1). The investigated sites in Sweden are all located some 100–200 km east of the highest mountains where ice growth presumably started during the glacial stages.

In or near the highest mountains in southern Norway, finds have been radiocarbon dated to MIS 3. Two musk ox bones, found in 1913 at Innset, Trøndelag (Fig. 1), have been radiocarbon-dated to about 38–40 cal ka BP (Hufthammer et al., 2019). Lie and Sandvold (1997) describe a sample of silty gyttja (organic sediment) imbedded in till in a lake sediment core from Bukkehåmmårtjørna in Jotunheimen, the region with the highest mountains in Scandinavia. They obtained two ^{14}C-dates on bulk gyttja that yielded 42 and 36 cal ka BP. Olsen et al. (2013) refer to two radiocarbon dates from a till section at Mesna (Fig. 1) that gave ages around 32 and 36 ka. However, these dates were obtained on bulk sediments with

Fig. 1. Map showing sites in the Nordic countries mentioned in the text. Red star shows the study site (Folldalen). Ålesund is the location for Skjonghelleren; Jotunheimen for Bukkhammartjønne; and Veiki moraine for the sites in Alexanderson et al. (2022).

low organic content (<2% TOC), and we do not consider them reliable. Lastly, Paus (2021) obtained an age of 44 cal ka BP from a small redeposited wood piece in a lake core from the Dovre mountains (Fig. 1). We decide in section 5.8 to reject such isolated old finite dates as listed here in our reconstructions, although accepting that some of them might be correct.

In the first part of this paper, we present ^{14}C- and luminescence-dating results that were obtained from exposed fine-grained, laminated (glaci-lacustrine) sediments situated underneath thick tills in Djupdalen, a ravine that ends in the valley Folldalen, south-east-Norway (Figs. 1 and 2, and S1). The site is located 550 m a.s.l. and close to the highest mountains (>2000 m) and near the former ice divide during the LGM. We therefore consider that the Scandinavian Ice Sheet must have been almost completely melted when these glaci-lacustrine sediments were deposited. We have given this ice-free period the informal name Folldalen interstadial.

In sections 5.5-5.6 we present a synthesis of the size of the entire Eurasian Ice Sheet Complex during Early MIS 3; in section 5.7 we compare the glacial fluctuations with the climate beyond the ice sheets; in section 5.8 we discuss the implication for the global sea-level changes, and in section 5.9 we modify a previously published glaciation curve for the western flank of the Scandinavian Ice Sheet.

2. Regional setting and earlier studies of the Djupdalen site in Folldalen

Djupdalen (English: The Deep Valley) is a small and narrow tributary valley to Folldalen, which is itself a tributary to Østerdalen (Figs. 2 and 3), the main south-draining valley in this easternmost part of southern Norway. During the last deglaciation, some 10.4 ka BP, the site was located 40–50 km south of the main water divide and the early LGM ice divide, and about the same distance north of the late LGM ice divide (Fig. 4). The latter ice sheet configuration led to the formation of a large ice-dammed lake between the ice divide and the water divide during the last deglaciation. Shorelines and glaciolacustrine sediments from this ice dammed lake are widespread in the area (Holmsen, 1915; Høgaas and Longva, 2018). The ice that blocked the southbound drainage, were small remnants located mainly in the valleys and they melted away within a few hundred years. We consider this as a model for our older glaci-lacustrine sediments.

Near the mouth of Djupdalen, there is a 20–30 m high cliff formed from massive, compact diamictons (Fig. 5), interpreted as basal tills by us and all earlier investigators (Thoresen and Bergersen, 1983). Below the till is a thick sequence of undisturbed laminated clay and silt with some sand layers, the age of which is the focus of the present study. The site was mentioned briefly by Holmsen (1915) and first described by Streitlien (1935) who concluded that the sub-till sediments are possibly of interglacial age. Only 1.3 km upstream from Djupdalen is another tributary creek, Gråmobekken (Fig. 3), from where a similar stratigraphy has been described. Streitlien (1935) described mainly the sediments at Gråmobekken, which had been exposed by a recent landslide.

Garnes (1978) also described the sediments at the Gråmobekken site and showed that the laminated sediments are very fine-grained with a clay content up to 95%. She stated that the

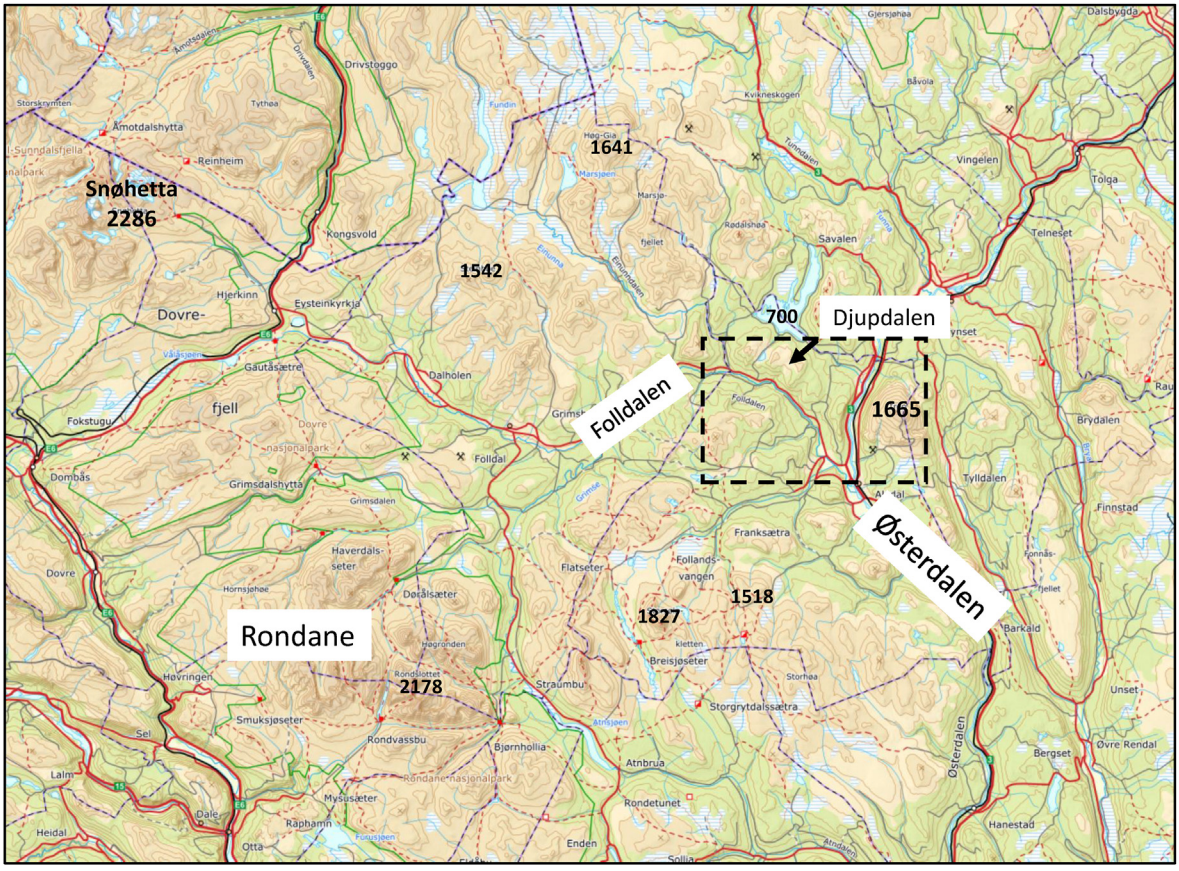

Fig. 2. Map of the area around Folldalen. The study site at Djupdalen is marked with an arrow and Fig. 3 with the dashed box. Altitudes (m a.s.l.) of some summits and one lake (700) are given with black numbers. Østerdalen is the main valley, through which the longest river in Norway, Glomma, flows southwards. Source: The Norwegian Mapping Authority.

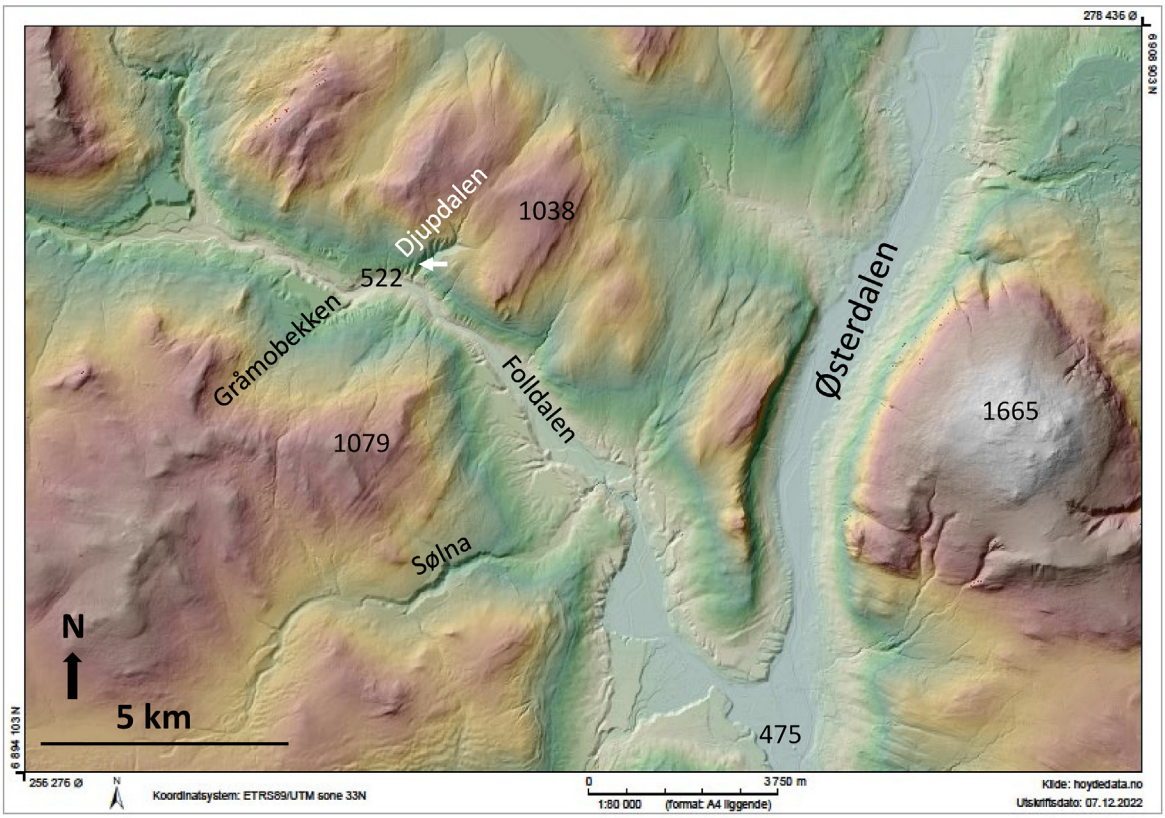

Fig. 3. Digital elevation model for Djupdalen and the surrounding area. The study site is marked with an arrow. Numbers give elevation in m a.s.l. for selected points. The mouth of Djupdalen is located 62.19 °N, 10.46 °E. Source: The Norwegian Mapping Authority.

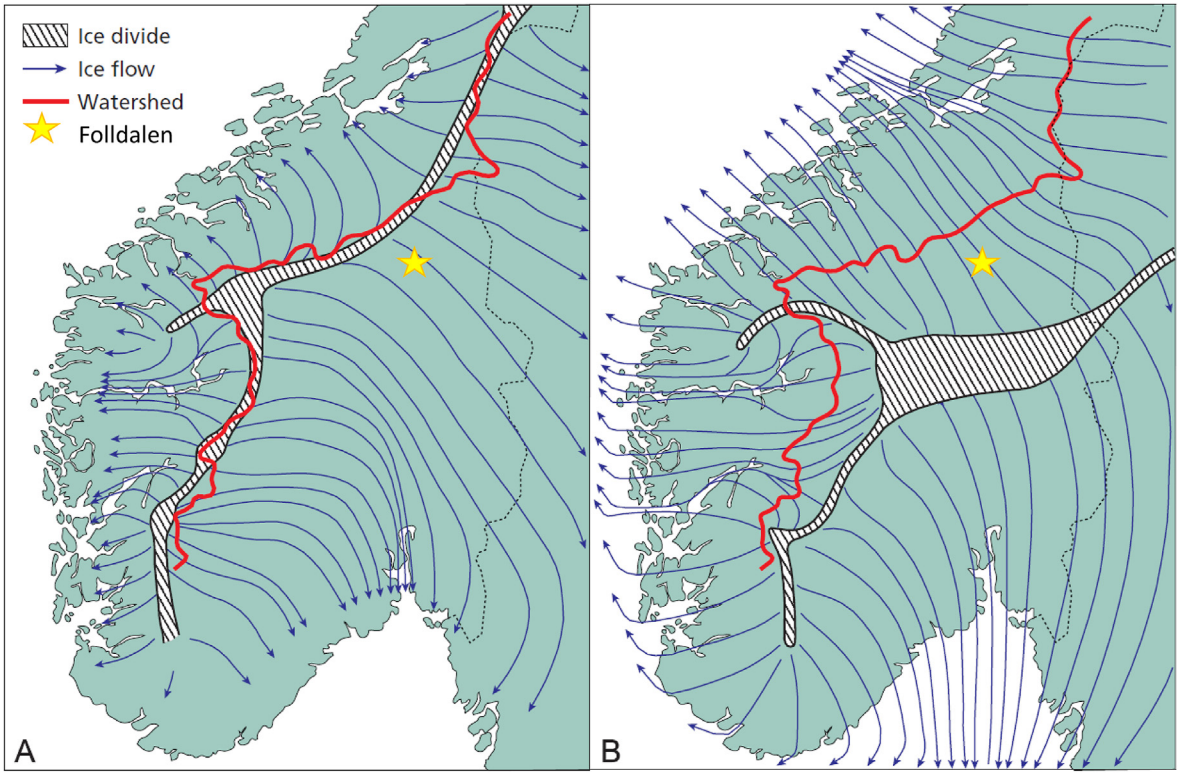

Fig. 4. Maps of southern Norway showing the present-day watershed in red. A) The ice divide and interpreted ice flow directions during an early phase of the LGM. B) The ice divides during a late phase of the LGM. Modified from Vorren and Mangerud (2008). The Dupdalen site in Folldalen is marked with a yellow star.

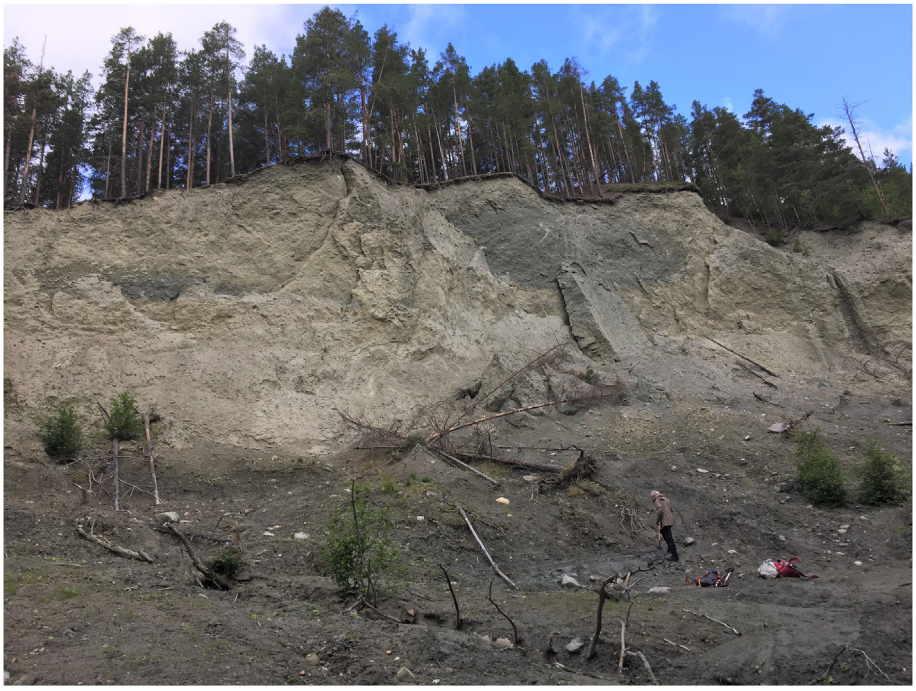

Fig. 5. Djupdalen. Photo taken towards the west. The wall consists of till beds. From the foot of the till wall there is a slope covered by slumped material down to the creek, which is located shortly below the photo. The man (JIS) is standing where we made the clearing D; the bedding in the silt is seen to left of his feet.

sediments are undoubtedly of glaciolacustrine origin and argued that their geographical/topographical position indicates that they were deposited during a deglaciation and not during an ice advance. The section at Gråmobekken is presently completely covered with slope material and has not been accessible to us.

Thoresen (1982) and Thoresen and Bergersen (1983) used an excavator to dig trenches down to bedrock, clarifying the full stratigraphy at both sites. At Gråmobekken, they found a 0.5 m thick sandy bed on the bedrock, covered by 20 m thick laminated clay and silt, which was overlain by a 20 m thick till and 20 m glacifluvial gravel on top. At Djupdalen, they found that a diamicton covering the bedrock is overlain by a 4-m-thick unit of sand and gravel followed by a 13-m-thick sequence of laminated silt and clay (Fig. 6). The top of the exposure consists of an about 25 m high cliff of basal tills. They present the result of three pollen samples, each with a pollen sum of about 225 pollen grains, which are dominated by grass and other herbs but have up to 30% birch, suggesting a sub-arctic vegetation. For two radiocarbon ages from organic matter in the gravelly unit at the base of the sequence at Gråmobekken, the NaOH-soluble fraction yielded an age of about 42 ka BP, and the non-soluble fraction about 37 cal ka BP (Table 1). They agreed with Garnes (1978) that the sediments must be of glaciolacustrine origin, but they imagined that the lake could have been dammed by an outlet glacier flowing down the Sølna Valley from the Rondane mountains.

Thoresen (1982) mapped glacial striae and till in a large area around Djupdalen, and found a sequence of ice-flow directions. The oldest was down the Folldalen valley, reflecting an initial build-up of ice in the high mountains with a valley glacier flowing down along Folldalen. The next flow direction was from the North-west, reflecting an ice divide located along the main water divide (Fig. 4). The last direction was from the South, showing that the ice divide had moved well to the south of the water divide (Fig. 4).

The latest study of the site was by Paus et al. (2011). They collected samples just below the till wall and considered them to be from glaci-lacustrine sediments. However, when we (Paus, Svendsen, Mangerud) visited the site in 2015 we found that they had probably sampled slumped material, possibly a mixture of the till and the sub-till sediments. They produced a pollen diagram with 6 samples (pollen sum 160–310), all showing similar assemblages to those of Thoresen and Bergersen (1983). They also obtained a radiocarbon age from plant macrofossils of about 35 cal ka BP (Table 1). It was in fact their finding of plant macrofossils for radiocarbon dating that inspired us to initiate the present study.

3. Methods

3.1. Field work

As mentioned above, in Djupdalen there is a vertical wall of till some 20–30 m high (Fig. 5). From the foot of the wall and down to the creek there is a gentle slope of slumped material that covers the sub-till glaci-lacustrine sediments, which can be seen in only a few places. One of us (JM) has visited the site several times since 1959, partly together with the late geologist O.F. Bergersen. We therefore knew the site and the stratigraphy well enough that we could confidently restrict the field work to areas where the landslide deposits were so thin that we could expose the sub-till sediments by hand.

We collected samples in sealed plastic bags for C-14 dating in 2015. Samples for luminescence dating were obtained by hammering in PVC tubes in 2020. Samples 2020–1 to –5 were taken with 5 cm diameter tubes. However, these tubes became deformed during hammering, and the rest were therefore taken with stronger 11 cm diameter PVC tubes. All tubes were 20 cm long, but a few broke during sampling.

Details of the sampling sites are given in the Supplementary. Some photos of the sediments and sampling sites are shown in Fig. 7.

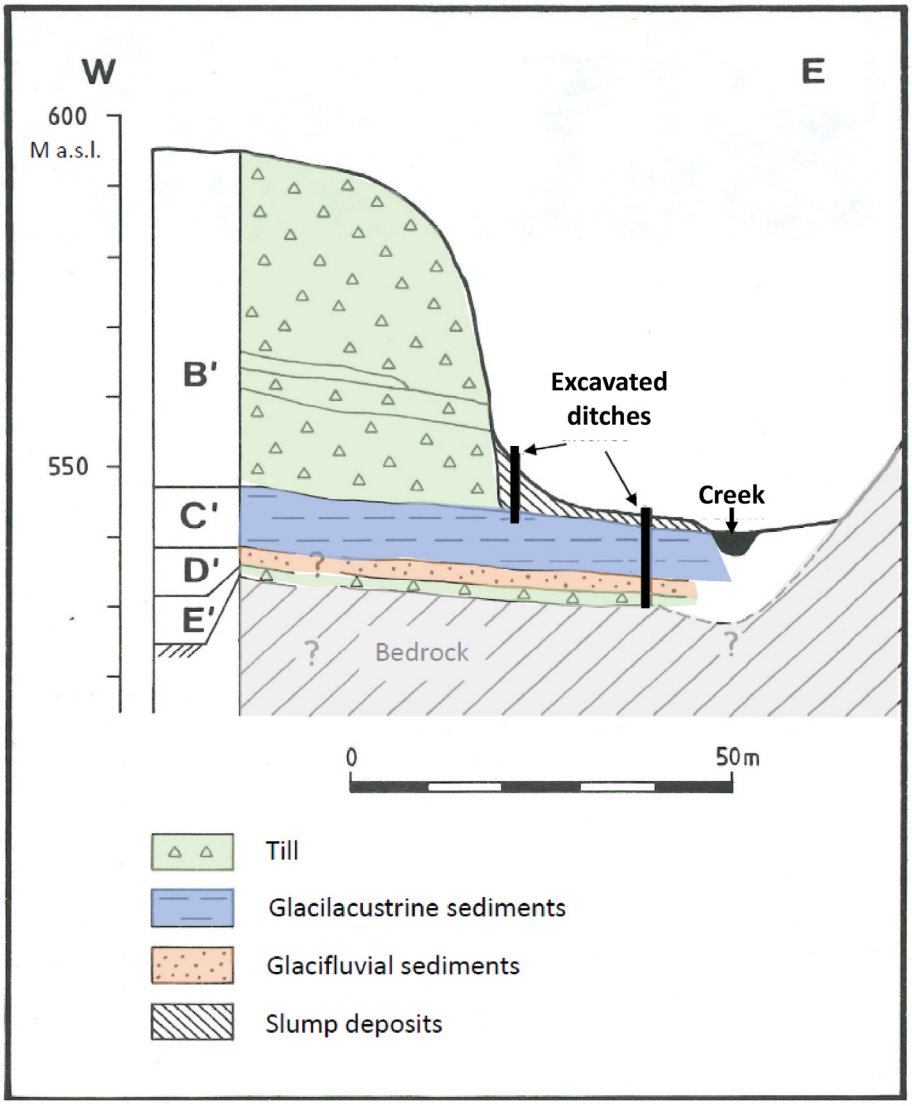

Fig. 6. The stratigraphy in Djupdalen is shown as a cross section of the valley according to Thoresen and Bergersen (1983). The black bars show their machine excavations. The sub-till sediments are also preserved in some places on the east valley slope – not shown in the profile.

3.2. Radiocarbon dating

Samples were taken from the sites A-9, C-13, and D-17 (Fig. S1). Sediment was suspended in water and washed through a 125 μm sieve. The residues were examined systematically under a stereo-microscope, and organic remains were picked out into water. These remains were again selected and picked out into water (rinsing). They were then picked out into a dry plastic box, gathered in a clump, and left to air-dry under a loose-fitting lid. The dry remains were weighed and transferred to a sterile vial for radiocarbon dating by the Poznan Radiocarbon Dating Laboratory, Poland. The procedure is described fully by Lotter and Birks (2020). After chemical treatment the samples were divided into two parts by the dating laboratory, A and B, which were dated separately (Table 1).

The organic particles were very small (<1 mm). They consisted mostly of unidentifiable leaf fragments and fragmented moss. Terrestrial mosses were used in the dating samples. The most frequent taxa were *Polytrichum, Dicranaceae* spp., *Aulacomnium turgidum, Racomitrium*, and *Bryum*. The other taxa identified are listed in Table 1.

3.3. Luminescence dating

The eighteen sampling tubes (Table S1) were opened and processed under darkroom conditions at the Lund Luminescence Laboratory, Lund University, Sweden. A brief description of the procedure is given here, for details see Supplementary material. Silty-sandy laminae were mainly targeted for sub-sampling for dose determination (Fig. S2) and material both from the sandy beds and from the surrounding silty clay was used to determine water content and sediment dose rate. From the eighteen tubes, twenty samples were taken for dating analysis. The 90–180 μm or 180–250 μm fraction was treated with 10% HCl, 10% H_2O_2 and 10–40% HF as well as density separated at 2.62 g/cm^3 and 2.58 g/cm^3 (LST Fastfloat) to extract clean quartz and K-feldspar grains.

Measurement of the equivalent dose was carried out in Risø TL/OSL readers model DA-20. The quartz grains were measured as large (8-mm) aliquots and with Single Aliquot Regeneration (SAR) protocols with post-IR blue stimulation (Murray and Wintle, 2003; Roberts and Wintle, 2001), the settings of which were determined based on preheat plateau, dose recovery tests and linear-modulated optically stimulated luminescence (LM-OSL) measurements

Table 1
Radiocarbon dates from Folldalen.

Field sample		Lab ID	^{14}C age	±1σ	TPM[a]	C[b]	Calibrated age					Dated material (Ref.)
							Median	68%		95%		
Djupdalen-			yr BP	yr	mg	mg C		min	max	Min	Max	
A-9	A	Poz-76999	38,900	1400	3.7	0.3	42,800	41,980	43,860	40,100	43,860	Juncus seed, leaf fragments of
	B	Poz-77000	35,900	1100		0.3	40,770	39,990	41,830	38,530	42,360	Salix herbacea, leaf and seed of Saxifraga oppositifolia, terrestrial moss. (This paper).
C-13	A	Poz-77001	>44,000		0.75	0.6	>46,250					Selaginella megaspore,
	B	Poz-77002	35,200	1300		0.2	40,030	39,030	41,660	37,140	42,140	Gnaphalium norvegicum fruit, Saxifraga oppositifolia and Salix leaf fragments, Salix bud, S. oppositifolia seed, Coenoccum geophilum sclerotia, terrestrial moss. (This paper).
D-17	A	Poz-78093	>46,000		0.4	0.6	>46,000					Selaginalla megaspore, Batrachium seed, Papaver seed, Salix bracts, Cenococcum geophilum sclerotia, Selaginella megaspore, leaf fragments, terrestrial moss. (This paper).
	B	Poz-78055	Modern			0.08	Modern					One piece, oviously a root. (This paper).
Site C		Poz-27215	30,810	370	24	2.0	35,170	34,710	35,490	34,510	35,990	Betula nana catkin scale, Salix budscale, seeds/megaspores of Empetrum. Silene dioica, Selaginella. (Paus et al., 2011)
Gråmobekken		T-3556 A	37,330	640			41,900	41,560	42,280	41,100	42,500	NaOH-dissolved.
		T-3556 B	32,520	650			37,060	36,110	38,010	35,640	39,060	Not dissolved. (Thoresen and Bergersen, 1983)

[a] TPM = Terrestrial plant material. Weighted.
[b] Dated mass of Carbon determined by CO_2 pressure.

(Figs. S3–S6). The fast ratio was calculated for all aliquots according to Durcan and Duller (2011). An infrared stimulated luminescence (IRSL) protocol with preheat 200 °C and infrared stimulation at 50 °C was used for small (2-mm) aliquots of K-feldspar from five samples (20071, −77, −79 A, −79 B, 80). For both quartz and feldspar, equivalent doses were calculated by exponential curve fitting in Risø Analyst v. 4.57. The mean dose recovery ratio for quartz OSL was 0.97 ± 0.04 (n = 41, OD = 17%), which shows that the analytical protocol can be used to successfully retrieve a given dose.

Field and saturated water content was determined by weighing. We used saturated water content (Table S2) for age determination; assuming the samples were below the ground water table until a few hundred years ago, when landslides had removed much of the overburden. The concentration of radionuclides in the sediment was determined by fusion ICP and ICP-MS at Actlabs, Canada (Table S3) and the internal K-content in the feldspar was assumed to be 12.5% (Huntley and Baril, 1997). Total environmental dose rates and ages were calculated in the DRAC online calculator (Durcan et al., 2015); mean doses were used for age calculation. Ages based on five or less accepted aliquots were considered unreliable.

Additionally, a synthetic sample consisting of all accepted aliquots was created and the Minimum Age Model (MAM) (Burow, 2021; Galbraith et al., 1999) was applied to its age distribution.

3.4. Pollen analyses

Sediment samples were extracted from cleaned profiles at sites A, B, C, and E. From these, eight pollen sub-samples (1 cm^3) were treated with HF and acetolysed following Fægri et al. (1989). We added *Lycopodium* tablets of known concentration to the samples to estimate pollen concentration (Stockmarr, 1971). In the pollen diagram (Fig. 8), the percentage calculation basis (ΣP) is the total sum of terrestrial pollen taxa. For a taxon X within aquatic plants (AQP), spores, and assumed reworked microfossils, the calculation basis is ΣP + X.

4. Results

We consider that the profile documented by Thoresen and Bergersen (1983) is representative for the main stratigraphy (Fig. 6), and that the laminated sub-till sediments were deposited in an ice-dammed lake during a short period during a deglaciation. As mentioned above we use the informal name Folldalen interstadial for the period when these sediments were deposited at Djupdalen and Gråmobekken. Details of our observations and sampling are given in the Supplementary Material.

The radiocarbon ages obtained are given in Table 1. Two yielded minimum ages >46 cal ka BP, whereas three gave finite ages 40–43 cal ka BP, and the last was a root giving modern age.

The quartz OSL ages are listed in Table 2. The quartz luminescence signal was dim (Fig. 9A), partly contaminated by feldspar and with a generally weak fast signal component (Fig. S2). Some aliquots also had high doses, possibly close to saturation ($D_e > 2D_0$). These non-ideal properties led to 71% of aliquots being rejected and relatively large uncertainties for individual samples (5–55% relative standard error; Table 2). The spread in ages is also large but 17 of the 20 samples gave ages in the range 50–75 ka, even considering the large spread in dose rate (Fig. 10). The mean age for all 20 samples is 66.5 ± 20.6 ka, and the weighted mean is 52.9 ± 4.0 ka. If we omit those samples considered as unreliable due to too few

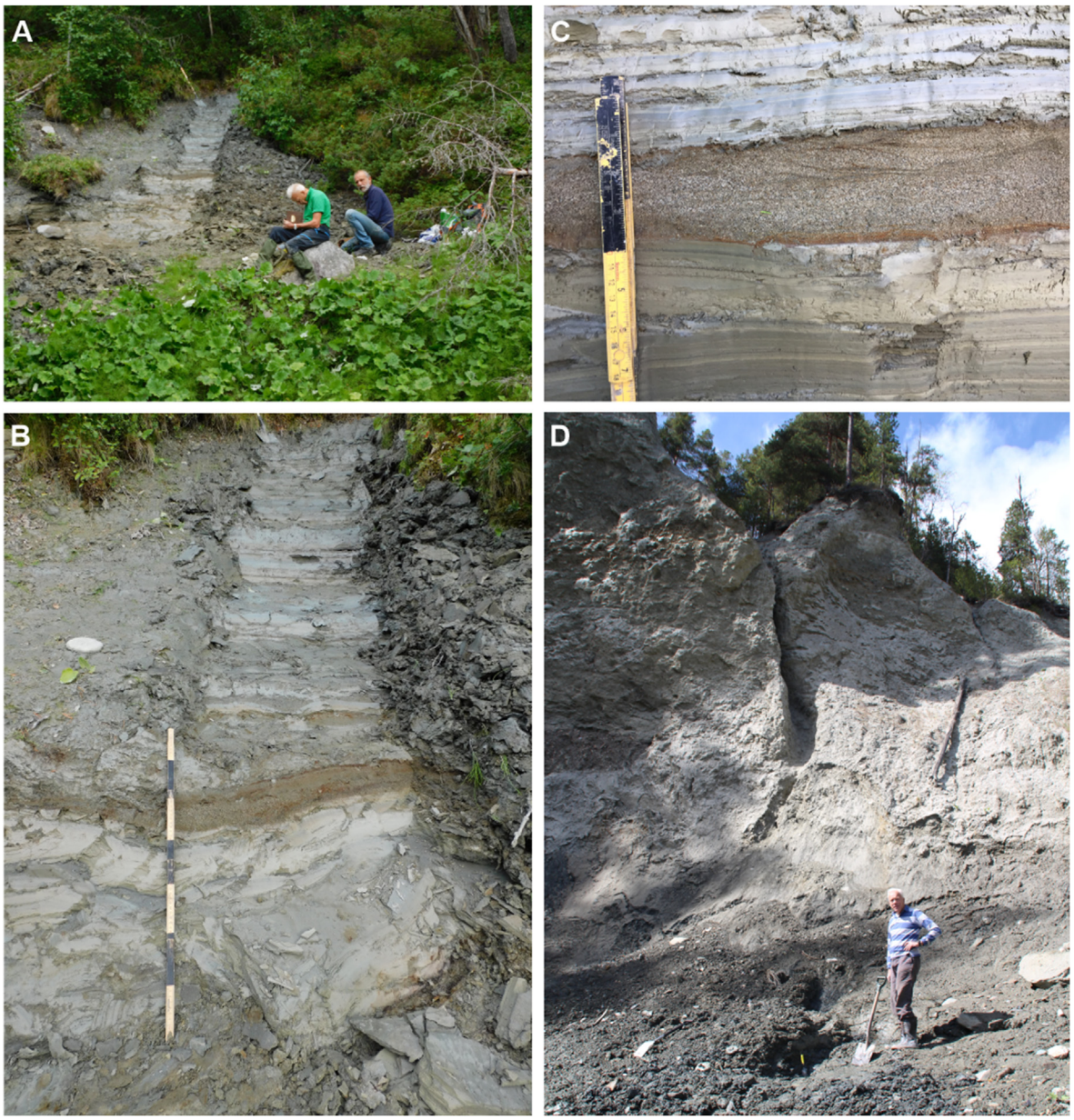

Fig. 7. A) Photo of the sequence at site A, the only excavation on the east side of the creek. B) Close-up photo of site A. The yellow and black markings on the ruler are 10 cm long. The thick brown sand bed is Sand 3. C) Sand bed 2 at site A. Note the current ripples. The shiny laminae consist of almost pure clay, whereas the brownish grey laminae are siltier. D) Unsuccessful attempts to excavate through the slumped material close to the till wall at site C. Paus et al. (2011) collected their samples near here.

aliquots (Table 2), the mean for the remaining 9 samples is 64.0 ± 16, and the weighted mean 53.8 ± 1.7 ka BP.

The feldspar IRSL ages are given in Table 3. In contrast to the quartz, the feldspar signal was bright, and it also continued to grow to high doses (Fig. 9B). All 5 samples gave ages >99 ka, that is much older than the quartz ages (Fig. 11). A stratigraphic overview of all luminescence samples is shown in Fig. S2, and additional luminescence data are presented in the Supplementary Material, including Figs. S3-S6 and Tables S2-S3.

The pollen results are shown in the diagram Fig. 8. Twenty-eight terrestrial and ten aquatic pollen and spore taxa were identified. Pollen concentrations are extremely low; maximum 4000 pollen grains cm^{-3} at site A and between 10 and 1000 at the other sites. The maximum pollen sum per sample is 75. The pollen assemblages are dominated throughout by herbs.

5. Discussion

5.1. Formation of the lake

We agree with all earlier authors, and with assessments made during several field excursions, that the silty-clayey sediments are ice-dammed lake deposits. The main argument is that it is almost impossible to envisage ways of damming a lake in this valley other than by glacial ice. We also find it most likely that the glaciolacustrine sediments were deposited during ice recession, in the same way as during the last deglaciation, as argued by Garnes (1978). Thoresen and Bergersen (1983) proposed that a valley glacier down the Sølna Valley could possibly form a dam at the mouth of Folldalen during the start of a glaciation (Fig. 3). We are sceptical about this possibility as we consider that an outlet glacier

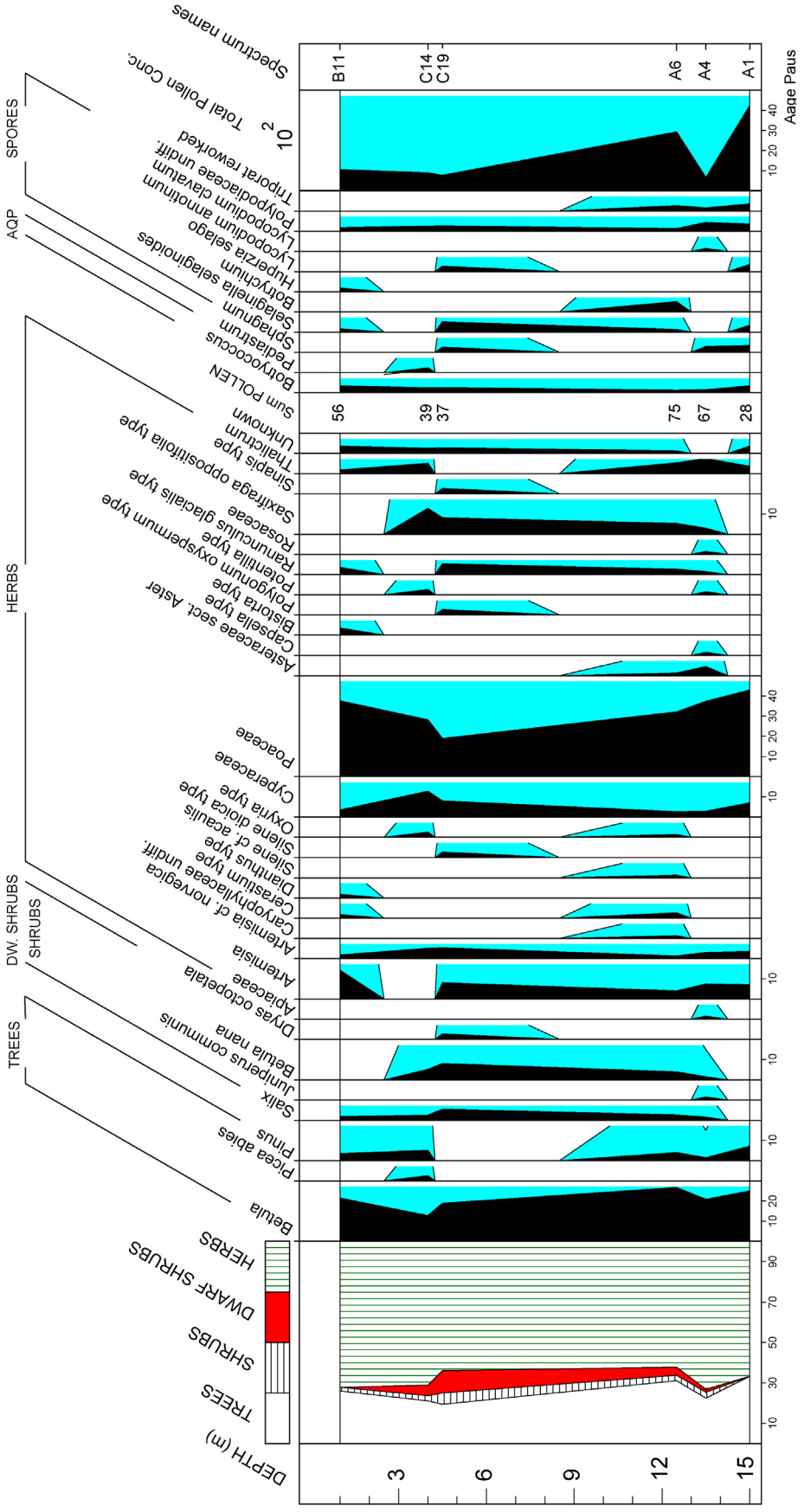

Fig. 8. Pollen percentage diagram from Djupdalen. Note that counted pollen per sample is only 28–75. Total pollen concentrations (grains per cm^3) are given on the right. Shaded curves are 10 x exaggerations of the scale. The zero point for the depth scale is 1 m above B11. The letters (A, B and C) in the spectrum names refer to our sites.

Table 2
Quartz luminescence data. For information on water content see Table S1, for radionuclide concentrations Table S2.

Bed	Sample no	Quartz age (ka)	Dose (Gy)	n	Dose rate (Gy/ka)	Comment
1	20071	50 ± 5	75.8 ± 7.2	10/32	1.52 ± 0.08	
2	20072	68 ± 10	100.1 ± 14.0	1/5	1.46 ± 0.08	Unreliable
2	20073	50 ± 9	73.0 ± 12.3	2/3	1.46 ± 0.08	Unreliable
2	20074 A	71 ± 13	98.8 ± 18.0	4/5	1.40 ± 0.07	Unreliable
2	20074 B	82 ± 10	114.1 ± 13.0	1/5	1.40 ± 0.07	Unreliable
2	20075	76 ± 6	108.8 ± 7.2	19/41	1.43 ± 0.07	
2	20076	73 ± 7	104.8 ± 8.8	6/21	1.43 ± 0.08	
2	20077	77 ± 10	95.7 ± 10.9	10/60	1.24 ± 0.06	
1	20078	125 ± 69	170.5 ± 93.6	2/13	1.36 ± 0.07	Unreliable
3	20079 A	66 ± 5	91.8 ± 4.7	13/24	1.39 ± 0.07	
3	20079 B	79 ± 11	110.2 ± 14.3	5/24	1.39 ± 0.07	Unreliable
4	20080	85 ± 10	108.7 ± 12.1	8/36	1.28 ± 0.07	
5	20082	54 ± 4	146.5 ± 8.2	6/36	2.69 ± 0.12	
5	20083	59 ± 9	159.4 ± 22.4	5/27	2.71 ± 0.12	
Silt (A)	20084	64 ± 7	185.9 ± 17.3	2/3	2.89 ± 0.13	Unreliable
Silt (A)	20085	26 ± 8	77.2 ± 22.0	1/3	2.93 ± 0.13	Unreliable
Silt (D)	20086	36 ± 3	109.4 ± 9.2	8/36	3.08 ± 0.15	
Silt (D)	20087	52 ± 12	156.9 ± 36.3	2/3	3.00 ± 0.14	Unreliable
Site X	20088	62 ± 4	184.3 ± 8.8	2/3	2.97 ± 0.13	Unreliable
Site X	20090	75 ± 9	220.7 ± 23.9	2/3	2.93 ± 0.13	Unreliable

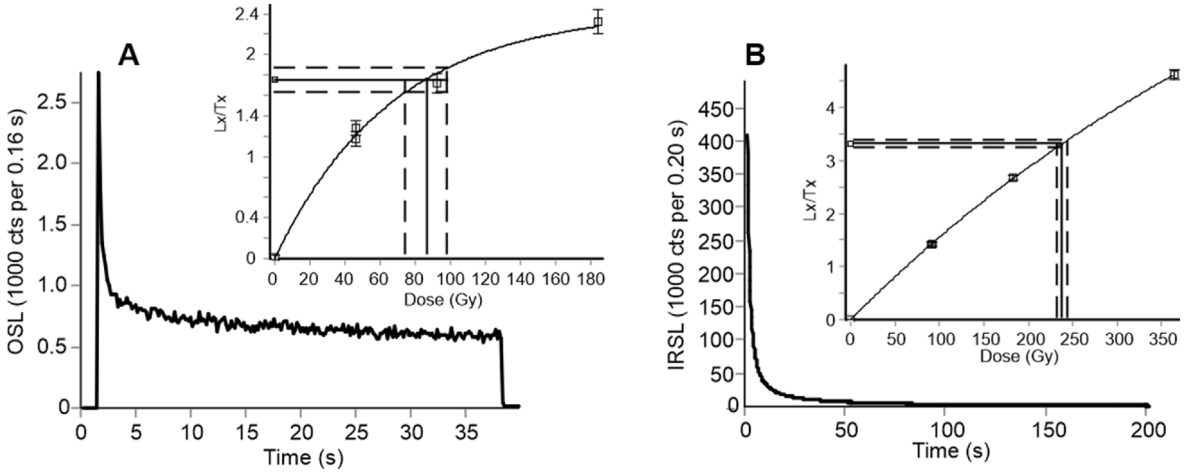

Fig. 9. Representative growth and decay curves from (A) quartz OSL and (B) K-feldspar IRSL50, both from sample 20,077.

Table 3
K-feldspar luminescence data.

Bed	Sample no	Feldspar age (ka)	Dose (Gy)	n	Dose rate (Gy/ka)
1	20071	105 ± 12	244.1 ± 22.7	6/6	2.33 ± 0.15
2	20077	99.2 ± 9.4	203.0 ± 13.4	3/3	2.05 ± 0.14
3	20079 A	113 ± 12	247.7 ± 21.3	6/6	2.20 ± 0.14
3	20079 B	135 ± 18	296.1 ± 34.1	6/6	2.20 ± 0.14
4	20080	161 ± 21	335.1 ± 38.5	6/6	2.08 ± 0.14

from an ice cap in the mountains would flow down the Folldalen valley before flowing down the Sølna Valley. However, the ice sheet configuration during formation of the lake is not crucial for our problem because 1) the thick overlying tills demonstrate that the lacustrine sediments pre-date the LGM and 2) it is clear from the geographic location that the Scandinavian Ice Sheet must have been almost gone when the lake existed based on the configurations during the LGM and the last deglaciation.

5.2. Vegetation

The pollen assemblages are dominated throughout by herbs (Fig. 8). *Saxifraga oppositifolia, Oxyria*, *Ranunculus glacialis*-type, and *Cerastium*-type indicate snow-bed vegetation, whereas *Artemisia norvegica*-type, *Dryas*, and *Silene acaulis*-type represent drought-tolerant vegetation on wind-blown ridges. Dominant grasses indicate open meadows with e.g., Caryophyllaceae, *Thalictrum*, and the pteridophytes *Selaginella* and *Botrychium*.

Betula nana, Salix, and *Juniperus* pollen show the presence of shrubs and dwarf-shrubs. Considering the local assemblage, *Pinus,* and probably also tree-birch (*Betula),* are interpreted as long-distance transported pollen.

In total, the pollen data reflect the presence of a sparse herb/dwarf-shrub tundra on basic soils. The presence of *Betula nana* and *Selaginella* indicate cool local summers with July minimum means of 7°C (Kolstrup, 1979). Since we assume that the sediments originate from a deglaciation period, the pollen assemblage would reflect a pioneer stage on immature soils rather than a climate maximum of an interstadial. Paus et al. (2011) presented similar pollen results from a sequence that is situated around the levels of site C. The pollen data of Thoresen and Bergersen (1983) from Djupdalsbekken and the adjacent Gråmobekken are also similar to our results.

The macrofossil assemblage, primarily identified for radiocarbon dating, confirms that the sediments are lacustrine, with

remains of *Batrachium* and aquatic mosses such as *Drepanocladus*. The terrestrial taxa indicate an arctic-alpine 'tundra' environment on immature base-rich soils. The commonest taxa are *Salix herbacea, Saxifraga oppositifolia,* and *Selaginella selaginoides* (see Table 1), and the mosses *Aulacomnium turgidum* and *Racomitrium*. Other taxa are *Gnaphalium norvegicum*, *Papaver, Juncus*, cf. *Sagina*, and *Polygonum viviparum*, and sclerotia of the mycorrhizal fungus *Coenococcum geophilum*.

5.3. Radiocarbon ages

We obtained six new radiocarbon dates from three samples. Three yielded calibrated ages in the range 40–43 ka BP, two gave non-finite ages >46 cal ka and the last was a modern root (Table 1). All samples, except the root, were dated on many small pieces of plant macrofossils. We expect that the real ages of all samples are within the error of radiocarbon ages.

We note that the two subsamples of each of the three samples gave significantly different ages, especially for D-17 where one subsample gave >46 ka and the other (a root) gave modern age. More interesting is sample C-13 where one subsample was dated to >46.2 ka and the other to 40 ka. The deviating results may indicate that we have dated plant fragments of mixed ages or, alternatively, that some fragments were contaminated with younger carbon. The two subsamples of A-9 also yielded ages that do not overlap within one standard deviation.

It is possible that the finite ages are correct and that the non-finite samples contained pieces that were redeposited from older deposits. It is noteworthy that finite radiocarbon ages were also obtained by Thoresen and Bergersen (1983) and Paus et al. (2011). However, contamination with only a tiny amount of younger carbon will produce such finite ages for infinitely old samples. We therefore favour the simpler explanation that the non-finite dates provided reliable minimum ages and that the samples giving finite ages were contaminated with younger carbon, an interpretation supported by our OSL dates. These differences demonstrate the difficulty of obtaining dating samples of minute fragments of plant material of ages close to or beyond the limit of radiocarbon dating.

5.4. OSL ages

In ice-dammed lake sediments there is a high-risk for incomplete bleaching, i.e. that the sediments were not exposed to sufficient sunlight for effective zeroing of the luminescence signals (Alexanderson and Murray, 2012; Fuchs and Owen, 2008; Thrasher et al., 2009). This explains the discrepancy between the quartz OSL ages and the feldspar IRSL ages (Murray et al., 2012; Möller and Murray, 2015), where the harder-to-bleach feldspar yields significantly older ages than the quartz, even without correcting for fading (Table 3, Fig. S2). The feldspar ages therefore do not represent the time of last deposition and we do not discuss them any further.

Since quartz bleaches faster than feldspar, the OSL ages are more likely to provide the correct age in a setting where light is limited, e.g. in turbid water (Bateman, 2019). Although the samples display largely similar ages despite large differences in dose rates (Fig. 10), even the quartz may be incompletely reset. The dim signals from the quartz, along with small amounts of material, unfortunately limit the ways in which we can investigate and potentially address the effect of incomplete bleaching for these samples, for example by applying statistical models such as the minimum age model (Galbraith et al., 1999) to large datasets. Small aliquots of this material do not provide sufficiently strong signal to be measured and the number of accepted aliquots per sample ($\leq$19) is too low to apply reliably statistical models (Rodnight, 2008).

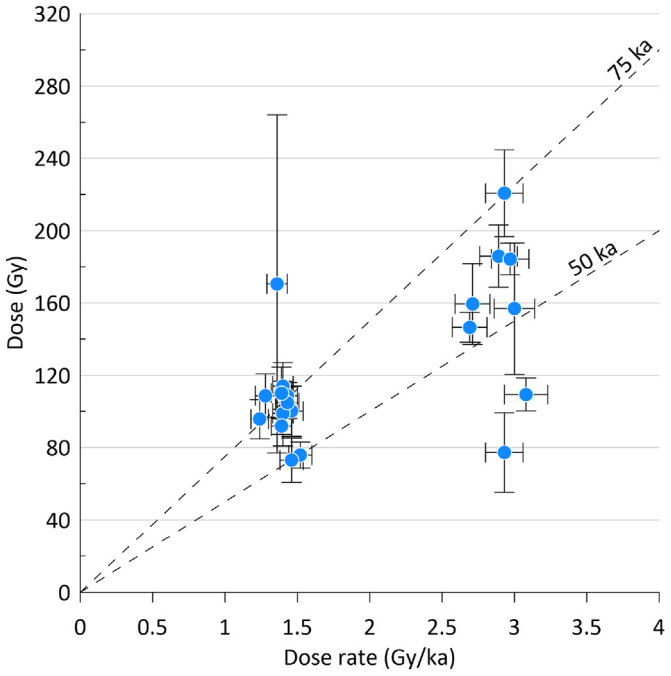

Fig. 10. Plot of quartz OSL dose vs environmental dose rate shows that ages scatter but most fall in the 75–50 ka age range, despite a large difference in dose rate (due to different nuclide concentrations in silt and sand; Table S2).

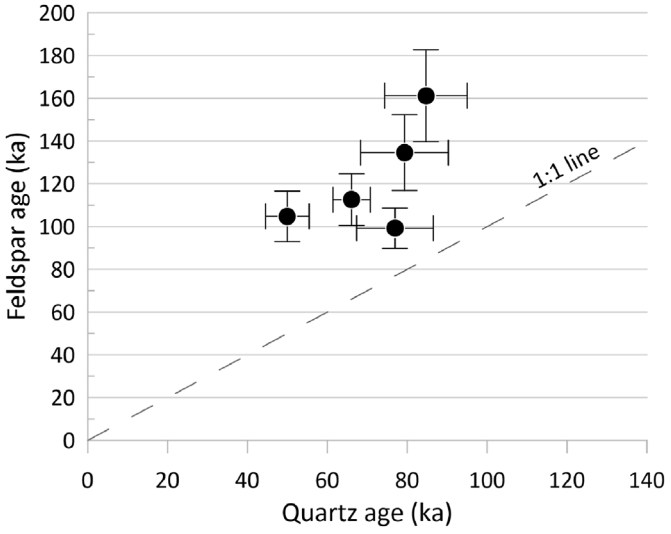

Fig. 11. Comparison of feldspar and quartz ages. For all samples where we have both types of ages, the feldspar ages are significantly higher than the quartz ages. This indicates that the dated sediment is incompletely bleached, in turn implying that the quartz age is most likely closest to the true age.

However, we treat the aliquots from all our samples as one synthetic small-aliquot dataset, which can be statistically analysed. It has been shown that in other sediment from the same region only 1% or less of grains give a luminescence signal (Alexanderson, 2022), meaning that our large ~1000-grain aliquots (180–250 μm) could be regarded as small aliquots, representing the signal from ~10 grains. Additionally, in our interpretation the sediments were deposited during some few hundred years (like in the analogue lake during the last deglaciation, see section 2), which, given the resolution of luminescence dating in this age range, is

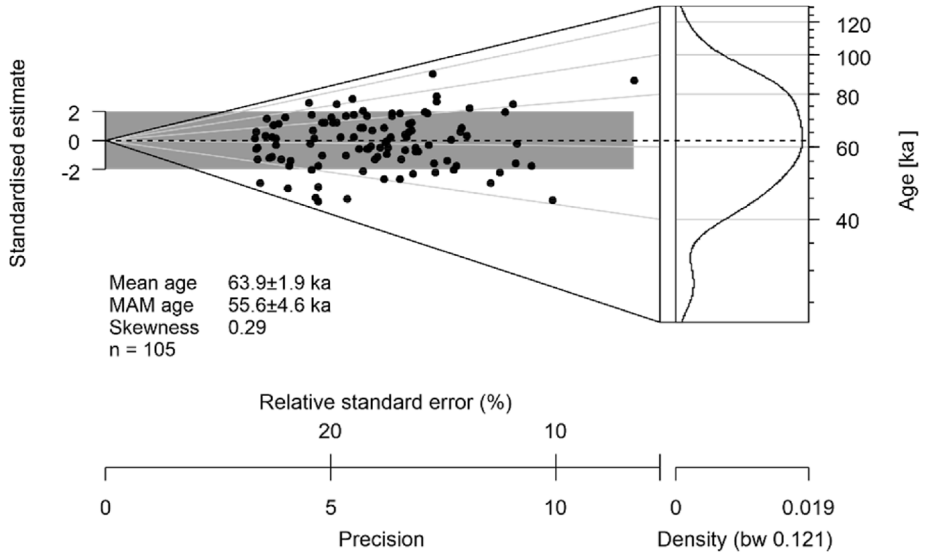

Fig. 12. Age distribution of the synthetic sample as well as the precision of individual aliquots as shown in an Abanico plot (Dietze et al., 2016). The distribution centres around 64 ka but applying a statistical age model (MAM) to account for incomplete bleaching (skewed age distribution) results in 55.6 ka as the preferred age.

considered to represent one and the same event and thus all aliquots can be combined into one sample (cf. Bateman et al., 2022).

The synthetic sample consists of 105 accepted aliquots (four outliers for this population removed according to the 1.5IQR rule) with a positively skewed age distribution (Fig. 12). Applying the minimum age model (Burow, 2021; Galbraith et al., 1999) to this dataset results in an age of 55.6 ± 4.6 ka (p = 0.05). We consider this age the best estimate of time of deposition from the luminescence data. This age has been calculated assuming water-saturated sediments since the time of deposition. If instead field water content (Table S2) is used, the age becomes younger (45.5 ± 3.5 ka). However, these sediments were deeply buried, and thus water-saturated, for most of the time since they were deposited.

The less-than-ideal luminescence characteristics of the quartz (dim signal, weak fast component; Fig. 9A and S4) could lead to incorrect ages due to e.g. influence from unstable signal components or poorly constrained equivalent doses (Bateman, 2019; Preusser et al., 2006). To optimize the signal, we have used early background subtraction (Cunningham and Wallinga, 2010) and rejected the aliquots with the lowest fast ratio (F < 5). That a correct dose can be recovered with the used protocol is shown by dose recovery tests that give results close to unity (mean ratio 0.97 ± 0.04), though the scatter is quite large (OD = 17%). The less-than-ideal luminescence properties are most likely connected to the local bedrock (Alexanderson, 2022), which is dominated by phyllites and mica schists (Norwegian-Geological-Survey, 2023). It is interesting to note that in nearby Rondane, just ~30 km to the SW of our site but in a different bedrock unit (i.e. sandstones), the quartz luminescence properties are much better (Bøe et al., 2007, Bøe pers. comm. 2005). This suggests that the material in Folldalen is mainly locally derived.

Based on our assessment of sedimentology (turbid water, fast deposition), quartz-feldspar age comparisons and dose distributions we conclude that the lake sediments were not exposed to enough light for complete bleaching of all luminescence signals. Additionally, the quartz luminescence characteristics are not ideal and lead to larger than usual uncertainties. Nevertheless, taking this into account we consider our best age estimate 55.6 ± 4.6 ka is a reliable age for the lake sediments. The age would be somewhat younger than 56 ka, and not older, if bleaching and/or water content were different from our assumptions.

5.5. The Scandinavian Ice Sheet during MIS 3

The most precisely dated MIS 3 interstadial in Scandinavia is probably the Ålesund interstadial, dated to 38-34 cal ka BP with almost 50 radiocarbon dates conducted mainly on bones (Mangerud et al., 2010). The ages correlate closely with Greenland interstadials 8 and 7. There are fewer dates around 36 ka BP, corresponding to Greenland stadial 8 (Svensson et al., 2008). The Ålesund interstadial sites are located along the west coast (Fig. 1) and thus do not imply a major inland retreat of the ice margin but the finds of reindeer bones (Valen et al., 1996) suggest that there were some larger areas of vegetation for grazing. Based on similar radiocarbon ages, the Ålesund interstadial is correlated with the Sandnes interstadial in south-western Norway (Fig. 1) (Raunholm et al., 2004). Thus, much of the west coast was ice free 38–34 ka BP, i.e. in the middle of MIS 3.

Directly underlying the Ålesund-interstadial beds are fine-grained, laminated, lacustrine sediments found in three marine-formed caves (Larsen et al., 1987; Valen et al., 1995) indicating that there have been lakes in the caves. These lakes could only have been formed if the cave openings were blocked by a glacier (during the Skjonghelleren advance, Fig. 13). A major paleomagnetic excursion is found in the lacustrine sediments at all three sites. It is correlated with the Laschamp excursion based on 1) the stratigraphic position directly below the 38 ka start of the Ålesund interstadial, 2) that the next major excursion back in time, the Blake, is about 115 ka (Osete et al., 2012) and 3) correlation with the Greenland ice core (Mangerud et al., 2003). The Laschamp excursion is dated to 40–42 ka BP (Cooper et al., 2021; Guillou et al., 2004), and thus the Skjonghelleren re-advance is also well dated. Therefore, there was at least one glacial re-advance that reached the outermost coast near Ålesund during MIS 3 (Fig. 1). This means that the Folldalen interstadial must have ended before 42 ka BP.

During the early Sandnes interstadial, correlated with the Ålesund interstadial (Raunholm et al., 2004), relative sea-levels reached an elevation of 200 m in SW Norway, strongly suggesting

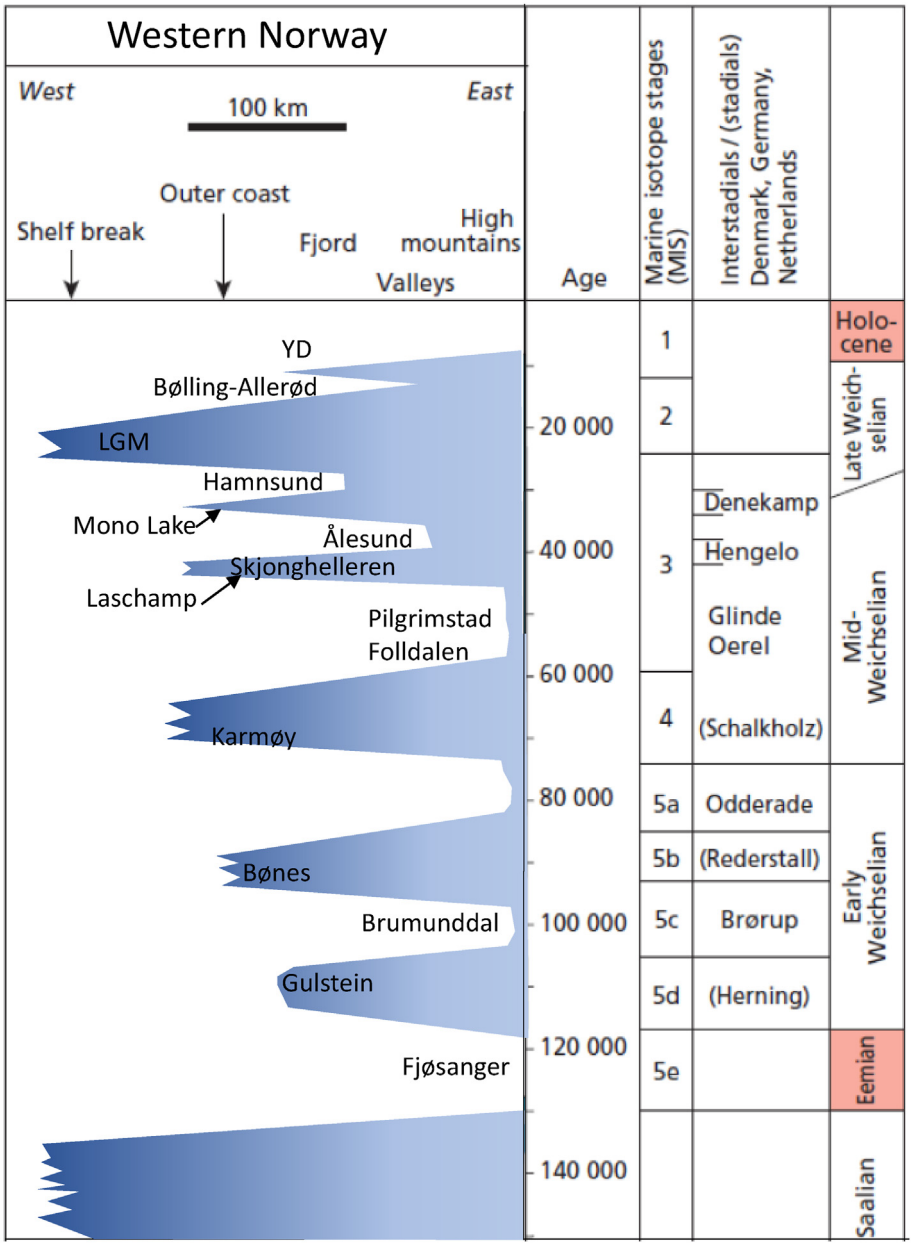

Fig. 13. A glaciation curve showing the fluctuations of the margin of the Scandinavian Ice Sheet in western Norway, modified from Mangerud et al. (2011). The main difference from earlier versions is that we now assume that the ice sheet melted away during the Folldalen interstadial, Early MIS 3. Names of (some) interstadials and glacial advances are marked. Also, the ages of the Laschamp and Mono Lake paleomagnetic excursions are marked.

a preceding major glaciation, which is then correlated with the Skjonghelleren re-advance (Sejrup et al., 2000). Sejrup et al. (2000) also assume that the Norwegian Channel Ice Stream was operating during the Skjonghelleren re-advance, implying ice over eastern Norway and western Sweden.

It is difficult to reconstruct the extent of the Skjonghelleren re-advance east of the main mountain chain. However, we postulate that all areas close to the high mountains were ice covered during the re-advance, an assumption supported by modelling (Patton et al., 2016). The implication is that if areas near the mountains were ice-free during MIS 3 that must have happened before and/or after the Skjonghelleren re-advance, about 41–42 ka BP.

We note that Wohlfarth (2010) and Kleman et al. (2021) extend the ice free period to 60–35 and 55–35 ka BP, respectively. The young end of their ice-free interval conflicts with the Skjonghelleren re-advance 41–42 ka. We cannot disprove them, but we adhere to the hypothesis of an ice advance 42–41 ka BP as we consider this glaciation is well dated in Norway.

Some sites in Scandinavia have one or two finite radiocarbon dates suggesting MIS 3 ages (Wohlfarth, 2010). However, these are close to the limit of the radiocarbon method, and we will not draw wide-ranging conclusions on these dates because such old dates are extremely sensitive to contamination with younger carbon. However, we accept that some of them might be correct. Other dating methods (OSL, amino acids, exposure dating) reach beyond the range of the radiocarbon method but often have real uncertainties larger than 10 ka (Alexanderson et al., 2014). The true age of the MIS 4/3 boundary is somewhat uncertain but is here

considered to be between 60–57 ka BP (Lisiecki and Stern, 2016). We infer that the areas discussed were ice covered during MIS 4, even though some dates suggest they were ice free.

We will next briefly consider some recent investigations close to the Scandinavian mountains that include a series of dates. Pilgrimstad in Central Sweden (Fig. 1) is a unique site because it contains rich finds of bones of mammoth, reindeer, and musk ox, and many other plant and animal remains. A review of earlier studies and the results of a thorough more recent study were presented by (Wohlfarth et al., 2011). The radiocarbon dates illustrate the problems with obtaining precise ages for MIS 3 sites. They listed 17 previously obtained finite radiocarbon ages in the range 26–52 ka BP, and 7 non-finite ages >35 to >40 ka. They reported 8 new radiocarbon dates; two gave finite ages in the MIS 3 range of 34 and 47 ka BP, whereas six yielded non-finite ages with some as old as >63 ka. They also reported 10 OSL ages (Alexanderson et al., 2010), where 9 yielded stratigraphically consistent ages in the range 36–49 ka and one from an older unit gave 74 ka. They describe several lithostratigraphic units but found no indications of a glacial advance, except a till on top. If the radiocarbon dates of >63 ka are correct, then the site pre-dates MIS 4. However, we consider this doubtful and place more emphasis on the OSL dates that consistently yielded Early MIS 3 ages.

Kleman et al. (2020) obtained 15 luminescence dates from the overrun Idre marginal moraine in Sweden located about 1000 m a.s.l. (Fig. 1). All, except two outliers, yielded ages in the range 58.8–52.9 with a mean of 55 ka. This correlates closely with our ages from Folldalen, but Folldalen must have been covered by ice when the Idre moraine was formed. Probably Folldalen is slightly younger than the Idre moraine. Kleman et al. (2020) also obtained ^{10}Be exposure ages and calculated that the ice-free period lasted about 20 ka, i.e. 55-35 ka. Möller et al. (2012) described sub-till sediments at Idre where 9 of the 10 samples cluster closely between 54 and 41 ka, with a mean of 45.6 ± 1.6 ka.

Alexanderson et al. (2022) provided 25 OSL dates for the overrun Veiki moraines in northern Sweden. The quartz had poor luminescence characteristics and there were problems with incomplete bleaching, but the results show clearly that the moraines are of MIS 3 age. The best estimate is that they were formed in few thousand years sometime in the time interval 56–39 ka.

We conclude that several sites, including Folldalen nearest to the high mountains, suggest that the Scandinavian Ice Sheet was small during an early part of MIS 3. The cited ages cover a considerable time range, about 35–58 ka BP. We cannot decide if this is due to imprecise ages, or if the dates represent two different ice-free periods interrupted by the Skjonghelleren re-advance, but we consider that the most extensive deglaciation took place during the Folldalen interstadial sometime between 48 and 60 ka BP.

5.6. MIS 3 ice retreat of other Eurasian ice sheets

In Svalbard, scientists have agreed for the last twenty years that there was a large MIS 4 glaciation and an early MIS 3 ice-free interstadial (Alexanderson et al., 2018; Ingólfsson and Landvik, 2013; Mangerud et al., 1998). The locality Kapp Ekholm is located only some 14 km away from a present-day tide-water glacier margin, and it is therefore postulated that when Kapp Ekholm was ice free there could not have been a large ice sheet covering Svalbard. The early MIS 3 age of the Kapp Ekholm interstadial is based on radiocarbon dates, luminescence dates and amino-acid chronology (Mangerud et al., 1998; Mangerud and Svendsen, 1992). This age was challenged by Eccleshall et al. (2016) who, based on quartz and feldspar luminescence ages, considered it more likely that the Kapp Ekholm interstadial is of MIS 5a age rather than MIS 3. However, they did not consider that the amino-acid chronology strongly suggests a MIS 3 age. We also note that they obtained 122 ± 9 ka for the Eemian interglacial at Kapp Ekholm with the IRSL method, which they accepted, and 52 ± 4 ka for the Kapp Ekholm interstadial with the same method.

We consider that the sites on Svalbard monitor the entire Svalbard-Barents Sea Ice Sheet; if an ice sheet covered the Barents Sea, it seems unlikely that much of Svalbard was ice free (Patton et al., 2016).

On Novaya Zemlya, amino-acid chronology, and also radiocarbon ages, suggest that it was ice-free during most of MIS 3 (Mangerud et al., 2008), although the dates and the high relative sea level suggest some glaciation during MIS 3. In the Polar Ural Mountains and other parts of Arctic Russia there were large ice sheets and ice caps during MIS 4 that disappeared during MIS 3 (Astakhov and Mangerud, 2012; Svendsen et al., 2004, 2019). However, there are also dates that may suggest that sizeable glaciers may have existed in the Polar Urals during parts of MIS 3 (Svendsen et al., 2019).

In Scotland the dating is apparently uncertain for some localities with till of probable MIS 4 age (Ballantyne et al., 2021). There are also some interstadial localities radiocarbon dated to about 35 ka (Finlayson et al., 2010). In the Scottish Highlands, considered to be the core area for glaciations, radiocarbon dates of bones from caves in the Assynt area give ages between 50–47 and 36-26 cal ka BP (Merritt et al., 2019). If southern Scandinavia was ice free, then the British Isles should also be ice free and the evidence from Scotland appears to support this.

In conclusion, evidence from all the Eurasian ice sheets, including our evidence from Folldalen, appears to show that the Eurasian Ice Sheet Complex was almost completely melted away sometime(s) during MIS 3 and most probably during the early part, 60–50 ka BP. There were probably some remnant ice caps and glaciers in mountains that holds glaciers today. We have schematically shown our interpretation in Fig. 14. The exact age and duration of that ice-free period cannot be determined based on the available results.

5.7. Vegetation and climate in europe beyond the ice sheets

It is well documented that the vegetation, and thus the summer climate in western Europe, fluctuated in parallel with the climate deduced from Greenland ice cores (Sánchez Goñi, 2022a; Sirocko et al., 2016). During Greenland interstadials much of Europe was forested, whereas during Greenland stadials, there was more cold-tolerant vegetation (Sánchez Goñi, 2022a). Ice sheets are mainly governed by winter precipitation and summer melting. The summer melting gives the fastest reaction of the ice front and thus on the areal extent, and a strong correlation between summer temperatures and glacier extent is well known.

Of special interest for the Scandinavian Ice Sheet are the results from the maars in the Eifel district in western Germany because this area is located only some 430 km SW of the LGM ice limit in Germany. Here Sirocko et al. (2016) recovered continuous stratigraphical sequences back to MIS 5e, partly annually laminated. They were able to tune the vegetation fluctuations with the Greenland stadials/interstadials. However, most interesting for the present paper is that Sirocko et al. (2016) found that the warmest conditions during MIS 3 occurred about 49–60 ka BP. During this period there were forests dominated by *Pinus* and *Picea* with considerable amounts of thermophilous trees such as *Ulmus* and especially *Carpinus* during the Early Weichselian interstadials. Based on seeds and other macrofossils from several species they concluded that the summer temperatures were only slightly cooler than today. After 49 ka BP the thermophilous trees declined and the vegetation became dominated by grass, suggesting a steppe

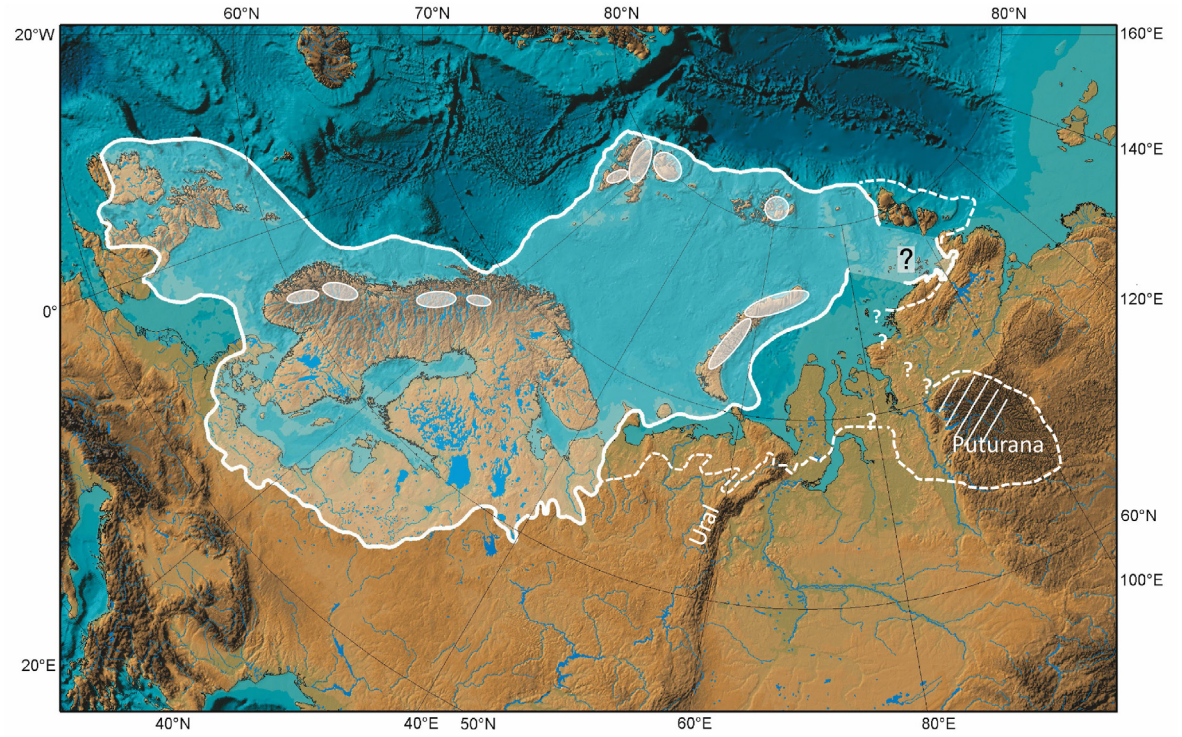

Fig. 14. A map showing the maximum extent of the Eurasian ice sheets during the LGM – full white line, from Svendsen et al. (2004). We have added schematically Early MIS 3 ice caps according to our interpretations (white ellipses), and our present opinion on the MIS 4 ice sheet limits in northern Russia and western Siberia (dashed line with question marks).

environment but there were still open *Betula-Pinus* forests during interstadials until about 36.5 ka BP. After this time trees were rare. We consider that these results are consistent with, and perhaps even support, our conclusion of an early MIS 3 ice-free period in Scandinavia.

There are also sites farther north where pollen stratigraphy implies a relatively warm climate during early MIS 3, although these sites do not contain as complete stratigraphy and precise dates as the Eifel maars. Sarala et al. (2016) described an exposure at Kaarreoja in Northern Finland with organic sediments below till. An OSL date from the lower part yielded 52 ka and radiocarbon dates from the upper gave 35 and > 45 ka BP. They found pollen and macrofossils of *Pinus* and tree *Betula*. Helmens et al. (2018) described an open tundra vegetation with *Betula*, *Pinus*, and *Picea,* at Sokli in northern Finland, and from chironomids and plant macrofossils they estimated that summer temperatures during early MIS 3 were only 1–2 °C cooler than at present. Hättestrand and Robertsson (2010) described birch forests during early MIS 3 at the Veiki sites in northern Sweden discussed in section 5.5. In Lake Yamosoro (65°01′N, 50°14′E) in northern Russia, Henriksen et al. (2008) reconstructed shrub tundra with open birch forest during early MIS 3.

The Scandinavian Ice Sheet was influenced by air masses from the North Atlantic Ocean, as was the vegetation in western Europe. The vegetation changes corresponded to the ocean climate fluctuations (van Kreveld et al., 2000) and the Greenland $\delta^{18}O$ curve during MIS 3 (Sánchez Goñi, 2022b; Sirocko et al., 2016). It is likely that the ice sheets also fluctuated in the same fashion, as both systems are sensitive to summer temperature. The postulated sensitivity is supported by the reactions of the ice sheet relative to the $\delta^{18}O$ variations in Greenland ice cores for the periods Bølling-Holocene, the Skjonghelleren-Ålesund interstadial, and the Hamnsund interstadial (Mangerud et al., 2010), and also by the results presented here for early MIS 3. Most glacial fluctuations are not dated precisely enough to detect short-term leads/lags. However, based on the reactions during Bølling-Younger Dryas, we assume that especially the western flank of the Scandinavian Ice Sheet was very climate sensitive.

5.8. Implication for the global eustatic sea-level curve

Several factors influence global sea level, but the large-amplitude fluctuations during the last glaciations are dominated by the total volume of glacial ice on land. Pico (2022) recently presented a compilation of sea-level curves for the last 120 ka (Fig. 15). The curves are based on different methods for estimating the sea level, and beyond the reach of the radiocarbon method, they are based on different dating methods. The curves are therefore different, both in the timing and amplitude of MIS 4–3 variations, but they have some main common features: 1) A low stand during MIS 4, for most curves at about −80 m. 2) A rise in sea level from MIS 4 to MIS 3 of 20–40 m, i.e., up to about −40 to −60 m. 3) A major sea-level fall to the LGM low stand at −116 to −128 m. We note that curves derived from glacial/GIA-modelling (Gowan et al., 2021; Pico et al., 2017) show a later MIS 3 high-stand than those based more directly on data.

There are several estimates of the volume of the Eurasian Ice Sheet Complex at the LGM and the corresponding sea-level equivalents. Hughes et al. (2016) used the relationship between area and volume of present-day glaciers and ice sheets, and concluded with about 24 m sea-level equivalents. Using glaciological modelling, Lambeck et al. (2010) found 21 m, Sejrup et al. (2022) 20 m, and Gowan et al. (2021) obtained the even lower number of 18.5 m. Here we note that Gowan et al. (2021) show a reduced (116 m) lowering during the LGM compared with most of the others (130 m).

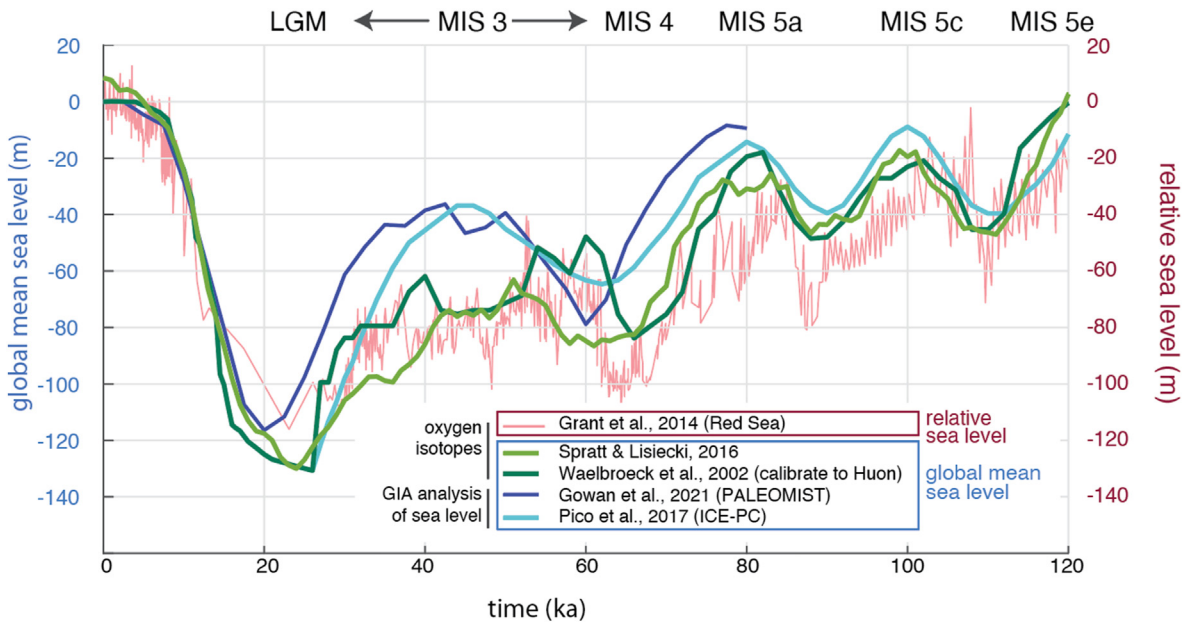

Fig. 15. Selected sea-level curves for the last 120 ka, simplified from a figure by Pico (2022). We consider that the melting of the Eurasian Ice Sheet Complex contributed to about 20 m of the sea-level rise from MIS 4 to MIS 3.

We argue that the volume of the Eurasian Ice Sheet Complex was approximately the same during MIS 4 as during the LGM (Gowan et al., 2021); it was slightly smaller in the west but considerably larger in northern Russia, as shown by Svendsen et al. (2004) (Fig. 14). However, Svendsen et al. (2004) apparently underestimated the MIS 4 extension on both sides of the Polar Urals (Svendsen et al., 2019), and it seems clear that the Putorana Plateau had a major ice cap during MIS 4 (Astakhov and Mangerud, 2012; Möller et al., 2019), possibly in contact with the Kara Ice Sheet (Astakhov and Nazarov, 2010) although this is disputed (Möller et al., 2019). The MIS 4 ice-extension across west Siberia is also somewhat controversial (Astakhov, 2017; Nazarov et al., 2022) but the Kara Ice Sheet hit the Taimyr Peninsula and covered the Severnaja Zemlya Islands towards the north-east (Fig. 14) (Möller et al., 2015).

If we accept that the Eurasian ice sheets contributed to about 20 m sea-level rise from MIS 4 to MIS 3, it would represent almost the entire rise for some reconstructions (Pico et al., 2017; Spratt and Lisiecki, 2016) shown in Fig. 15, and about half for the others (Gowan et al., 2021; Waelbroeck et al., 2002) except the one by Grant et al. (2014). The implication is that the other ice sheets, particularly the North American ice sheets, being much larger than the Eurasian ice sheets, decreased little in volume from MIS 4 to MIS 3. In contrast, the 20 m from the Eurasian ice sheets, constitutes less than one third of the global sea-level drop from MIS 3 to MIS 2, meaning that the North American ice sheets at that time expanded considerably.

The Red Sea sea-level reconstruction has a higher time resolution, and it suggests more fluctuations in ice-sheet volumes through MIS 3 than the other curves. Grant et al. (2012) reconstruct fast sea-level rise of more than 12 m ka^{-1} at the MIS 4/3 boundary, in their time scale at about 61.4 ka BP, at 37.5 ka BP, i.e. early in the Ålesund interstadial, and at the onset of the Holocene. During all three periods we have inferred fast retreat of the Scandinavian Ice Sheet, and probably the climate sensitive Scandinavian Ice Sheet was the main driver for the fast sea-level changes in both these and some other time intervals. We note that Gowan et al. (2021), in contrast, postulated that most sea-level fluctuations during MIS 3 were caused by the Laurentide Ice Sheet.

5.9. Glaciation curve for the Scandinavian Ice Sheet

We use the new dates from Folldalen to improve the glaciation curve of Mangerud et al. (2011) for western Norway (Fig. 13). The main modification is that we now assume that the ice sheet melted almost entirely during an early part of MIS 3.

After the Skjonghelleren re-advance (42–41 ka BP) came the Ålesund interstadial (Mangerud et al., 2010), which implies that at least the entire coast was ice free. This ice-free period is correlated with the Sandnes interstadial further south (Raunholm et al., 2004). There are a few dates from central Norway, for example from the musk ox bones mentioned in the introduction (Hufthammer et al., 2019), which also suggest a major retreat during the Ålesund interstadial. However, these are isolated finds where the age only relies on a few radiocarbon dates. So far, we have been reluctant to accept such a major retreat based these finds, but we cannot rule out the possibility that they are correct.

We consider that the western flank of the Scandinavian Ice Sheet was more climate sensitive than the eastern flank, meaning that ice-margin oscillations may have been more frequent and had larger amplitudes in the west than in the east. However, the large-scale development must be similar, and therefore the main features of the glaciation curve (Fig. 13) should be valid for the entire ice sheet – if they are correct for western Norway. An apparent conflict with our interpretation is the Ristinge glacial advance to Denmark, which Houmark-Nielsen (2010) dated to 50 ± 4 ka BP. However, if it could be as young as 42 ka it could correlate with the Skjonghelleren re-advance.

6. Conclusions

- Sub-till lake sediments in Folldalen, eastern Norway, were deposited in an ice-dammed lake in a valley located close to the highest mountains and close to the ice-divide during MIS 2.
- The best age estimate for the sediments is 55.6 ± 4.6 ka from 20 quartz OSL dates, which we consider to be a good approximation.
- The main conclusion is that sometime between 60–50 ka BP, during Early Marine Isotope Stage (MIS) 3, the Scandinavian Ice

Sheet melted completely. Local ice caps and glaciers could have persisted in the highest mountains.
- Pollen and macrofossil results suggests cool summers and a sparse arctic vegetation on well-drained ridges and in snowbeds.
- Our synthesis suggests that the entire Eurasian Ice Sheet Complex had melted away during Early MIS 3.
- This contributed about 24 m to sea-level rise, which is more than half of the eustatic sea-level rise from MIS 4 to MIS 3.
- If correct, the North American ice sheets did not decrease much in volume from MIS 4 to MIS 3.
- The Scandinavian Ice Sheet formed and melted away several times during the Last Ice Age, the Weichselian, corresponding to times of warmer interstadials in Greenland and western Europe.

Author contributions

Jan Mangerud: Conceptualization, field work, writing most of the manuscript, reviewing, editing. Helena Alexanderson: Responsible for the luminescence dating and writing the relevant sections. Hilary H. Birks: Picked material for radiocarbon dating from sediment samples and identified plant macrofossils. Aage Paus: Field work and pollen analyses. Zoran M. Perić;: Laboratory analyses for luminescence dating. John Inge Svendsen: Conceptualization, field work, funding. All co-authors: Contributed actively in the analyses of the reults and in the writing process.

Declaration of competing interest

The authors declare that they have no known competing financial interests or personal relationships that could have appeared to influence the work reported in this paper.

Data availability

All data are included in the paper.

Acknowledgements

The project was supported by the projects “Quantifying and understanding rates of ice sheet change (RISES)” and “Climate History of the Arctic Seaboard of Eurasia (CHASE)”, funded by the Bjerknes Centre for Climate Research and The Research Council of Norway (project no. 255415/E10), respectively. Jason Briner critically read the manuscript and suggested several improvements. The journal reviewers, Astrid Lysså and Henry Patton, also proposed important improvements.

Appendix A. Supplementary data

Supplementary data to this article can be found online at https://doi.org/10.1016/j.quascirev.2023.108136.

References

Alexanderson, H., 2022. Luminescence characteristics of Scandinavian quartz, their connection to bedrock provenance and influence on dating results. Quat. Geochronol. 69, 101272.
Alexanderson, H., Backman, J., Cronin, T.M., Funder, S., Ingólfsson, Ó., Jakobsson, M., Landvik, J.Y., Löwemark, L., Mangerud, J., März, C., Möller, P., O'Regan, M., Spielhagen, R.F., 2014. An Arctic perspective on dating Mid-Late Pleistocene environmental history. Quat. Sci. Rev. 92, 9–31.
Alexanderson, H., Henriksen, M., Ryen, H.T., Landvik, J.Y., Peterson, G., 2018. 200 ka of glacial events in NW Svalbard: an emergence cycle facies model and regional correlations. Arktos 4, 3.
Alexanderson, H., Hättestrand, M., Lindqvist, M.A., Sigfúsdóttir, T., 2022. MIS 3 age of the Veiki moraine in N Sweden – dating the landform record of an intermediate-sized ice sheet in Scandinavia. Arctic Antarct. Alpine Res. 54, 239–261.
Alexanderson, H., Johnsen, T., Murray, A.S., 2010. Re-dating the Pilgrimstad Interstadial with OSL: a warmer climate and a smaller ice sheet during the Swedish Middle Weichselian (MIS 3)? Boreas 39, 367–376.
Alexanderson, H., Murray, A.S., 2012. Problems and potential of OSL dating Weichselian and Holocene sediments in Sweden. Quat. Sci. Rev. 44, 37–50.
Astakhov, V., Mangerud, J., 2012. The chronology of the last ice age on the lower yenissei. Dokl. Earth Sci. 455, 219–222.
Astakhov, V., Nazarov, D., 2010. Correlation of upper pleistocene sediments in northern west Siberia. Quat. Sci. Rev. 29, 3615–3629.
Astakhov, V.I., 2017. A new model of Pleistocene glaciation in the northern Urals. Dokl. Earth Sci. 476, 1200–1202.
Ballantyne, C.K., Hall, A.M., Dawson, A.G., 2021. The quaternary in Scotland. In: Ballantyne, C.K., Gordon, J.E. (Eds.), Landscapes and Landforms of Scotland. Springer International Publishing, pp. 53–96.
Bateman, M.D., 2019. Applications in glacial and periglacial environments. In: Bateman, M.D. (Ed.), Handbook of Luminescence Dating. Whittles Publishing, Dunbeiath, pp. 191–221.
Bateman, M.D., Bryant, R.G., Luo, W., 2022. Getting the right age? Testing luminescence dating of both quartz and feldspars against independent age controls. Quat. Geochronol. 72, 101366.
Burow, C., 2021. calc_MinDose( ): apply the (un-)logged minimum age model (MAM) after Galbraith et al. (1999) to a given De distribution. Function version 0.4.4. In: Kreutzer, S., Burow, C., Dietze, M., Fuchs, M.C., Schmidt, C., Fischer, M., Friedrich, J., Mercier, N., Riedesel, S., Autzen, M., Mittelstrass, D., Gray, H.J. (Eds.), Luminescence: Comprehensive Luminescence Dating Data Analysis. R package version 0.9.11.
Bøe, A.-G., Murray, A., Dahl, S.O., 2007. Resetting of sediments mobilised by the LGM ice-sheet in southern Norway. Quat. Geochronol. 2, 222–228.
Cooper, A., Turney, C.S.M., Palmer, J., Hogg, A., McGlone, M., Wilmshurst, J., Lorrey, A.M., Heaton, T.J., Russell, J.M., McCracken, K., Anet, J.G., Rozanov, E., Friedel, M., Suter, I., Peter, T., Muscheler, R., Adolphi, F., Dosseto, A., Faith, J.T., Fenwick, P., Fogwill, C.J., Hughen, K., Lipson, M., Liu, J., Nowaczyk, N., Rainsley, E., Bronk Ramsey, C., Sebastianelli, P., Souilmi, Y., Stevenson, J., Thomas, Z., Tobler, R., Zech, R., 2021. A global environmental crisis 42,000 years ago. Science 371, 811–818.
Cunningham, A.C., Wallinga, J., 2010. Selection of integration time intervals for quartz OSL decay curves. Quat. Geochronol. 5, 657–666.
Dalton, A.S., Pico, T., Gowan, E.J., Clague, J.J., Forman, S.L., McMartin, I., Sarala, P., Helmens, K.F., 2022. The marine δ18O record overestimates continental ice volume during Marine Isotope Stage 3. Global Planet. Change 212, 103814.
Dietze, M., Kreutzer, S., Burow, C., Fuchs, M., Fischer, M., Schmidt, C., 2016. The abanico plot: visualising chronometric data with individual standard errors. Quat. Geochronol. 31, 12e18. https://doi.org/10.1016/j.quageo.2015.09.003.
Durcan, J.A., Duller, G.A.T., 2011. The fast ratio: a rapid measure for testing the dominance of the fast component in the initial OSL signal from quartz. Radiat. Meas. 46, 1065–1072.
Durcan, J.A., King, G.E., Duller, G.A.T., 2015. DRAC: dose rate and age calculator for trapped charge dating. Quat. Geochronol. 28, 54–61.
Eccleshall, S.V., Hormes, A., Hovland, A., Preusser, F., 2016. Constraining the chronology of pleistocene glaciations on svalbard: Kapp Ekholm re-visited. Boreas 45, 790–803.
Finlayson, A., Merritt, J., Browne, M., Merritt, J., McMillan, A., Whitbread, K., 2010. Ice sheet advance, dynamics, and decay configurations: evidence from west central Scotland. Quat. Sci. Rev. 29, 969–988.
Fuchs, M., Owen, L.A., 2008. Luminescence dating of glacial and associated sediments: review, recommendations and future directions. Boreas 37, 636–659.
Fægri, K., Iversen, J., Kaland, P., Krzywinski, K., 1989. Text Book of Pollen Analyses, 4. revised edition. Wiley, Chichester.
Galbraith, R.F., Roberts, R.G., Laslett, G.M., Yoshida, H., Olley, J.M., 1999. Optical dating of single and multiple grains of quartz from Jinmium rock shelter, northern Australia. Part I: experimental design and statistical models. Archaeometry 41, 339–364.
Garnes, K., 1978. Zur Stratigraphie der Weichseleiszeit im zentralen Südnorwegen. In: Nagel, H. (Ed.), Beiträge zur Quartär- und Landschaftsforschung. Ferdinand Hirt, Wien, pp. 195–220.
Gowan, E.J., Zhang, X., Khosravi, S., Rovere, A., Stocchi, P., Hughes, A.L.C., Gyllencreutz, R., Mangerud, J., Svendsen, J.-I., Lohmann, G., 2021. A new global ice sheet reconstruction for the past 80 000 years. Nat. Commun. 12, 1199.
Grant, K.M., Rohling, E.J., Bar-Matthews, M., Ayalon, A., Medina-Elizalde, M., Ramsey, C.B., Satow, C., Roberts, A.P., 2012. Rapid coupling between ice volume and polar temperature over the past 150,000 years. Nature 491, 744–747.
Grant, K.M., Rohling, E.J., Ramsey, C.B., Cheng, H., Edwards, R.L., Florindo, F., Heslop, D., Marra, F., Roberts, A.P., Tamisiea, M.E., Williams, F., 2014. Sea-level variability over five glacial cycles. Nat. Commun. 5, 5076.
Guillou, H., Singer, B.S., Laj, C., Kissel, C., Scaillet, S., Jicha, B.R., 2004. On the age of the Laschamp geomagnetic excursion. Earth Planet Sci. Lett. 227, 331–343.
Helmens, K.F., Katrantsiotis, C., Kuosmanen, N., Luoto, T.P., Salonen, J.S., Väliranta, M., 2018. Prolonged interglacial warmth during the last glacial in northern Europe. Boreas 167, 61–73.
Henriksen, M., Mangerud, J., Matiouchkov, A., Murray, A.S., Paus, A., Svendsen, J.I., 2008. Intriguing climatic shifts in a 90 kyr old lake record from northern Russia. Boreas 37, 20–37.

Holmsen, G., 1915. Brædæmte sjøer i Nordre Østerdalen. Norges geologiske undersøkelse 73.
Houmark-Nielsen, M., 2010. Extent, age and dynamics of marine Isotope stage 3 glaciations in the southwestern baltic basin. Boreas 39, 343–359.
Hufthammer, A.K., Nesje, A., Higham, T.F.G., 2019. Radiocarbon dates of two musk ox vertebrae reveal ice-free conditions during late Marine Isotope Stage 3 in central South Norway. Palaeogeogr. Palaeoclimatol. Palaeoecol. 524, 62–69.
Hughes, A.L.C., Gyllencreutz, R., Lohne, Ø.S., Mangerud, J., Svendsen, J.I., 2016. The last Eurasian ice sheets – a chronological database and time-slice reconstruction, DATED-1. Boreas 45, 1–45.
Huntley, D., Baril, M., 1997. The K content of the K-feldspars being measured in optical dating or in thermoluminescence dating. Ancient TL 15, 11–13.
Hättestrand, M., Robertsson, A.-M., 2010. Weichselian interstadials at Riipiharju, northern Sweden; interpretation of vegetation and climate from fossil and modern pollen records. Boreas 39, 296–311.
Høgaas, F., Longva, O., 2018. The early Holocene ice-dammed lake Nedre Glomsjø in Mid-Norway: an open lake system succeeding an actively retreating ice sheet. Norw. J. Geol. 98, 661–675.
Ingólfsson, Ó., Landvik, J.Y., 2013. The Svalbard–Barents Sea ice-sheet – historical, current and future perspectives. Quat. Sci. Rev. 64, 33–60.
Kleman, J., Hättestrand, M., Borgström, I., Fabel, D., Preusser, F., 2021. Age and duration of a MIS 3 interstadial in the Fennoscandian Ice Sheet core area – implications for ice sheet dynamics. Quat. Sci. Rev. 264, 107011.
Kleman, J., Hättestrand, M., Borgström, I., Preusser, F., Fabel, D., 2020. The Idre marginal moraine – an anchorpoint for Middle and Late Weichselian ice sheet chronology. Quaternary Science Advances 2, 100010.
Kolstrup, E., 1979. Herbs as july temperature indicators for parts of the pleniglacial and lateglacial in The Netherlands. Geol. Mijnbouw 58, 377–380.
Lambeck, K., Purcell, A., Zhao, J., Svensson, N.-O., 2010. The scandinavian ice sheet: from MIS 4 to the end of the last glacial maximum. Boreas 39, 410–435.
Larsen, E., Gulliksen, S., Lauritzen, S.-E., Lie, R., Løvlie, R., Mangerud, J., 1987. Cave stratigraphy in western Norway; multiple Weichselian glaciations and interstadial vertebrate fauna. Boreas 16, 267–292.
Lie, Ø., Sandvold, S., 1997. Late Weichselian—Holocene Glacier and Climate Variations in Eastern Jotunheimen, South-Central Norway. Department of Geography. University of Bergen.
Lisiecki, L.E., Stern, J.V., 2016. Regional and global benthic δ18O stacks for the last glacial cycle. Paleoceanography 31, 1368–1394.
Lotter, A.F., Birks, H.H., 2020. Sampling protocol for AMS radiocarbon dating of terrestrial plant macrofossils | Ecological and Environmental Change. Research Group | UiB.
Mangerud, J., Dokken, T., Hebbeln, D., Heggen, B., Ingólfsson, O., Landvik, J.Y., Mejdahl, V., Svendsen, J.I., Vorren, T.O., 1998. Fluctuations of the Svalbard-Barents Sea Ice sheet during the last 150 000 years. Quat. Sci. Rev. 17, 11–42.
Mangerud, J., Gulliksen, S., Larsen, E., 2010. ^{14}C-dated fluctuations of the western flank of the Scandinavian Ice Sheet 45-25 kyr BP compared with Bølling-Younger Dryas fluctuations and Dansgaard-Oeschger events in Greenland. Boreas 39, 328–342.
Mangerud, J., Gyllencreutz, R., Lohne, Ø., Svendsen, J.I., 2011. Glacial history of Norway. In: Ehlers, J., Gibbard, P., Hughes, P. (Eds.), Quaternary Glaciations - Extent and Chronology. Elsevier, Amsterdam, pp. 279–298.
Mangerud, J., Kaufman, D., Hansen, J., Svendsen, J.I., 2008. Ice-free conditions in Novaya Zemlya 35 000-30 000 cal years B.P., as indicated by radiocarbon ages and amino acid racemization evidence from marine molluscs. Polar Res. 27, 187–208.
Mangerud, J., Løvlie, R., Gulliksen, S., Hufthammer, A.-K., Larsen, E., Valen, V., 2003. Paleomagnetic correlations between scandinavian ice-sheet fluctuations and Greenland dansgaard-oeschger events, 45,000-25,000 yrs B.P. Quat. Res. 59, 213–222.
Mangerud, J., Svendsen, J.I., 1992. The last interglacial-glacial period on Spitsbergen, Svalbard. Quat. Sci. Rev. 11, 633–664.
Merritt, J.W., Hall, A.M., Gordon, J.E., Connell, E.R., 2019. Late Pleistocene sediments, landforms and events in Scotland: a review of the terrestrial stratigraphic record. In: Earth and Environmental Science. Transactions of the Royal Society of Edinburgh, pp. 1–53.
Miller, G.H., Andrews, J.T., 2019. Hudson Bay was not deglaciated during MIS-3. Quat. Sci. Rev. 225, 105944.
Murray, A.S., Thomsen, K.J., Masuda, N., Buylaert, J.P., Jain, M., 2012. Identifying well-bleached quartz using the different bleaching rates of quartz and feldspar luminescence signals. Radiat. Meas. 47, 688–695.
Murray, A.S., Wintle, A.G., 2003. The single aliquot regenerative dose protocol: potential for improvements in reliability. Radiat. Meas. 37, 377–381.
Möller, P., Alexanderson, H., Funder, S., Hjort, C., 2015. The Taimyr Peninsula and the Severnaya Zemlya archipelago, Arctic Russia: a synthesis of glacial history and palaeo-environmental change during the Last Glacial cycle (MIS 5e–2). Quat. Sci. Rev. 107, 149–181.
Möller, P., Anjar, J., Murray, A.S., 2012. An OSL-dated sediment sequence at Idre, west-central Sweden, indicates ice-free conditions in MIS 3. Boreas 42, 25–42.
Möller, P., Benediktsson, Í.Ö., Anjar, J., Bennike, O., Bernhardson, M., Funder, S., Håkansson, L.M., Lemdahl, G., Licciardi, J.M., Murray, A.S., Seidenkrantz, M.-S., 2019. Glacial history and palaeo-environmental change of southern Taimyr Peninsula, arctic Russia, during the middle and late pleistocene. Earth Sci. Rev. 196, 102832.
Möller, P., Murray, A.S., 2015. Drumlinised glaciofluvial and glaciolacustrine sediments on the Småland peneplain, South Sweden – new information on the growth and decay history of the Fennoscandian Ice Sheets during MIS 3. Quat. Sci. Rev. 122, 1–29.
Nazarov, D.V., Nikolskaia, O.A., Zhigmanovskiy, I.V., Ruchkin, M.V., Cherezova, A.A., 2022. Lake yamal, an ice-dammed megalake in the west siberian arctic during the late pleistocene, ~60–35 ka. Quat. Sci. Rev. 289, 107614.
Norwegian-Geological-Survey, 2023. B e d r o c k - National bedrock database. https://geo.ngu.no/kart/berggrunn_mobil/.
Olsen, L., Sveian, H., Ottesen, D., Rise, L., 2013. Quaternary glacial, interglacial and interstadial deposits of Norway and adjacent onshore and offshore areas. In: Olsen, L., Fredin, O., Olesen, O. (Eds.), Quaternary Geology of Norway, pp. 79–144.
Osete, M.-L., Martín-Chivelet, J., Rossi, C., Edwards, R.L., Egli, R., Muñoz-García, M.B., Wang, X., Pavón-Carrasco, F.J., Heller, F., 2012. The Blake geomagnetic excursion recorded in a radiometrically dated speleothem. Earth Planet Sci. Lett. 353–354, 173–181.
Patton, H., Hubbard, A., Andreassen, K., Winsborrow, M., Stroeven, A.P., 2016. The build-up, configuration, and dynamical sensitivity of the Eurasian ice-sheet complex to Late Weichselian climatic and oceanic forcing. Quat. Sci. Rev. 153, 97–121.
Paus, A., 2021. Lake Heimtjønna at Dovre, Mid-Norway, reveals remarkable late-glacial and Holocene sedimentary environments and the early establishment of spruce (Picea abies), alder (Alnus cf. incana), and alpine plants with present centric distributions. Quat. Int. 580, 38–52.
Paus, A., Velle, G., Berge, J., 2011. The Lateglacial and early Holocene vegetation and environment in the Dovre mountains, central Norway, as signalled in two Lateglacial nunatak lakes. Quat. Sci. Rev. 30, 1780–1796.
Pico, T., 2022. Toward new and independent constraints on global mean sea-level highstands during the last glaciation (marine Isotope stage 3, 5a, and 5c). Paleoceanogr. Paleoclimatol. 37, e2022PA004560.
Pico, T., Creveling, J.R., Mitrovica, J.X., 2017. sea-level records from the U.S. Mid-atlantic constrain Laurentide ice sheet extent during marine Isotope stage 3. Nat. Commun. 8, 15612.
Preusser, F., Ramseyer, K., Schlüchter, C., 2006. Characterisation of low OSL intensity quartz from the New Zealand Alps. Radiat. Meas. 41, 871–877.
Raunholm, S., Larsen, E., Sejrup, H.P., 2004. Weichselian interstadial sediments on Jaeren (SW Norway) - paleoenvironments and implications for ice sheet configuration. Norw. J. Geol. 84, 91–106.
Roberts, H.M., Wintle, A.G., 2001. Equivalent dose determinations for polymineralic fine-grains using the SAR protocol: application to a Holocene sequence of the Chinese Loess Plateau. Quat. Sci. Rev. 20, 859–863.
Rodnight, H., 2008. How many equivalent dose values are needed to obtain a reproducible distribution? Ancient TL 26, 3–9.
Sánchez Goñi, M.F., 2022a. Chapter 2 - the climatic and environmental context of the Late Pleistocene. In: Romagnoli, F., Rivals, F., Benazzi, S. (Eds.), Updating Neanderthals. Academic Press, pp. 17–38.
Sánchez Goñi, M.F., 2022b. The climate and environmental context of the Late Pleistocene. In: Romagnoli, F., Rivals, F., Benazzi, S. (Eds.), Updating Neanderthals. Elsevier, Amsterdam, pp. 17–38.
Sarala, P., Väliranta, M., Eskola, T., Vaikutiené, G., 2016. First physical evidence for forested environment in the Arctic during MIS 3. Sci. Rep. 6, 29054.
Sejrup, H.P., Hjelstuen, B.O., Patton, H., Esteves, M., Winsborrow, M., Rasmussen, T.L., Andreassen, K., Hubbard, A., 2022. The role of ocean and atmospheric dynamics in the marine-based collapse of the last Eurasian Ice Sheet. Communications Earth & Environment 3, 119.
Sejrup, H.P., Larsen, E., Landvik, J., King, E.L., Haflidason, H., Nesje, A., 2000. Quaternary glaciations in southern Fennoscandia: evidence from southwestern Norway and the northern North Sea region. Quat. Sci. Rev. 19, 667–685.
Sirocko, F., Knapp, H., Dreher, F., Förster, M.W., Albert, J., Brunck, H., Veres, D., Dietrich, S., Zech, M., Hambach, U., Röhner, M., Rudert, S., Schwibus, K., Adams, C., Sigl, P., 2016. The ELSA-Vegetation-Stack: reconstruction of Landscape Evolution Zones (LEZ) from laminated Eifel maar sediments of the last 60,000 years. Global Planet. Change 142, 108–135.
Spratt, R.M., Lisiecki, L.E., 2016. A Late Pleistocene sea level stack. Clim. Past 12, 1079–1092.
Stockmarr, J., 1971. Tablets with spores in absolute pollen analysis. Pollen Spores 13, 615–621.
Streitlien, I., 1935. De løse avleiringer. I W. Marlow: foldal. Norges geologiske undersøkelse 145, 26–64.
Svendsen, J.I., Alexanderson, H., Astakhov, V.I., Demidov, I., Dowdeswell, J.A., Funder, S., Gataullin, V., Henriksen, M., Hjort, C., Houmark-Nielsen, M., Hubberten, H.W., Ingólfson, O., Jakobsson, M., Kjær, K., Larsen, E., Lokrantz, H., Lunkka, J.P., Lysså, A., Mangerud, J., Matiouchkov, A., Murray, A., Möller, P., Niessen, F., Nikolskaya, O., Polyak, P., Saarnisto, M., Siegert, C., Siegert, M., Spielhagen, R., Stein, R., 2004. Late quaternary ice sheet history of northern Eurasia. Quat. Sci. Rev. 23, 1229–1271.
Svendsen, J.I., Færseth, L.M.B., Gyllencreutz, R., Haflidason, H., Henriksen, M., Hovland, M.N., Lohne, Ø.S., Mangerud, J., Nazarov, D., Regnéll, C., Schaefer, J.M., 2019. Glacial and environmental changes over the last 60 000 years in the Polar Ural Mountains, Arctic Russia, inferred from a high-resolution lake record and other observations from adjacent areas. Boreas 48, 407–431.
Svensson, A., Andersen, K., Bigler, M., Clausen, H., Dahl-Jensen, D., Davies, S., Johnsen, S., Muscheler, R., Parrenin, F., Rasmussen, S., Röthlisberger, R., Seierstad, I., Steffensen, J.P., Vinther, B., 2008. A 60 000 year Greenland stratigraphic ice core chronology. Clim. Past 4, 47–57.
Thoresen, M., 1982. Morenestratigrafi I Folldal, Hedmark. Department of Geology.

University of Bergen, p. 183. + 100 illustrations.
Thoresen, M., Bergersen, O., 1983. Submorene sedimenter i folldal, hedmark. Norges geologiske undersøkelse 389, 37–55.
Thrasher, I.M., Mauz, B., Chiverrell, R.C., Lang, A., 2009. Luminescence dating of glaciofluvial deposits: a review. Earth Sci. Rev. 97, 145–158.
Valen, V., Larsen, E., Mangerud, J., 1995. High-resolution paleomagnetic correlation of Middle Weichselian ice-dammed lake sediments in two coastal caves, western Norway. Boreas 24, 141–153.
Valen, V., Larsen, E., Mangerud, J., Hufthammer, A.K., 1996. Sedimentology and stratigraphy in the cave Hamnsundhelleren, western Norway. J. Quat. Sci. 11, 185–201.
van Kreveld, S., Sarnthein, M., Erlenkeuser, H., Grootes, P., Jung, S., Nadeau, M.J., Pflaumann, U., Voelker, A., 2000. Potential links between surging ice sheets, circulation changes, and the Dansgaard-Oeschger Cycles in the Irminger Sea, 60–18 Kyr. Paleoceanography 15, 425–442.
Vorren, T., Mangerud, J., 2008. Glaciations come and go. Pleistocene, 2.6 million-11,500 years ago. Pp. 480-533. In: Ramberg, I., Bryhni, I., Nøttvedt, A., Rangnes, K. (Eds.), The making of a land - Geology of Norway. Norsk Geologisk Forening, Trondheim.
Waelbroeck, C., Labeyrie, L., Michel, E., Duplessy, J.C., McManus, J.F., Lambeck, K., Balbon, E., Labracherie, M., 2002. Sea-level and deep water temperature changes derived from benthic foraminifera isotopic records. Quat. Sci. Rev. 21, 295–305.
Wohlfarth, B., 2010. Ice-free conditions in Sweden during marine oxygen Isotope stage 3? Boreas 39, 377–398.
Wohlfarth, B., Alexanderson, H., Ampel, L., Bennike, O., Engels, S., Johnsen, T., Lundqvist, J., Reimer, P., 2011. Pilgrimstad revisited – a multi-proxy reconstruction of Early/Middle Weichselian climate and environment at a key site in central Sweden. Boreas 40, 211–230.